Review Article

Mohammednoor Altarawneh*, Niveen W. Assaf, Hamed M. Hussain, and Bogdan Z. Dlugogorski

Structural properties of alumina surfaces and their roles in the synthesis of environmentally persistent free radicals (EPFRs)

https://doi.org/10.1515/ntrev-2022-0536 received May 4, 2022; accepted March 14, 2023

Abstract: Alumina oxides have been widely utilised as independent catalysts or as support materials for other catalysts. From an environmental perspective, alumina nanoclusters dispersed on surfaces of particulate matter PM₁₂, generated from various combustion processes, play a critical role in the synthesis of environmentally persistent free radicals (EPFRs). Of particular importance are phenoxy-type EPFRs that often act as building blocks for the formation of notorious pollutants. Herein, we present a systematic review of the literature pertinent to structural features of alumina surfaces at the nano-scale and their well-established role in the synthesis of EPFRs. Central to the capacity of alumina surfaces in mediating the formation of EPFRs are their active Lewis acid-base sites. The nature of these sites is very sensitive to hydration scenarios. As evident in electroparamagnetic resonance measurements, more than one category of EPFR forms on alumina surfaces. This generally entails the coexistence of various surface terminations, varying degrees of hydrations, and distinct underlying reaction pathways. The mechanisms for the formation of EPFRs over alumina surfaces involve interactions with terminal OH groups followed by creating genuine chemical bonds with Al³⁺ sites. Higher concentrations of EPFRs were often detected on

alumina surfaces, in reference to other transition metal oxides. We envisage that future studies may focus on the generation of EPFRs from potential precursors other than phenols and catechol, such as brominated species and substituted thiophenols.

Keywords: alumina, phenoxy radical, surfaces, free radicals, mechanisms

1 Introduction

Owing to their mesoporous structures, high surface areas, and profound chemical and thermal stability, aluminabased materials have been widely used as catalyst supports in a wide array of applications ranging from reforming reactions to hydro-desulphurisation [1]. However, stand-alone alumina surfaces also mediate the formation of an emerging class of pollutants: the environmentally persistent free radicals (EPFRs). The interest in studying EPFRs originates from their toxic attributes. They induce significant oxidative stress and have been identified in various environmental matrices, most notably, the particulate matter [2]. Halogenated/hydroxylated benzenes, phenols, and polycyclic aromatic hydrocarbons serve as precursors for EPFRs. During the incineration of municipal wastes, the concentration of these species may reach up to $1,000 \,\mu\text{g/m}^3$ [3]. In the cooling zone of municipal waste incinerators (MSWIs), metal oxides, typically dispersed on alumina and iron oxides serve as catalytic surfaces in the synthesis of EPFRs via complex physisorption and chemisorption processes [4]. Electronic paramagnetic resonance (EPR) measurements have unequivocally pinpointed the electronic nature of various oxygen- and carbon-centred EPFRs [5].

The high concentrations of alumina in MSWIs render it an important catalyst in the surface-assisted formation of EPFRs and the notorious dioxin-like compounds. The concentration of alumina in fly ash can reach up to 25–30 wt% [6]. In the cooling zone of MSWI, the alumina

Niveen W. Assaf: Department of Chemical Engineering, Faculty of Engineering Technology, Al Balqa Applied University, Al-Salt, 19117, Iordan

Hamed M. Hussain: Department of Chemical and Petroleum Engineering, United Arab Emirates University, Al-Ain 15551, United Arab Emirates

Bogdan Z. Dlugogorski: Energy and Resources Institute, Charles Darwin University, Darwin, NT 0909, Australia

^{*} Corresponding author: Mohammednoor Altarawneh, Department of Chemical and Petroleum Engineering, United Arab Emirates University, Al-Ain 15551, United Arab Emirates,

e-mail: mn.altarawneh@uaeu.ac.ae

surface can be present as a mixture of hydrated and dehydrated configurations. Hence, the lower- and higher-temperature ends of the cooling zone involve the hydrated and dehydrated surfaces of alumina. A few mechanistic studies have revealed the effect of surface termination and atomic dopants on pathways that underline the formation of EPFRs [7–9].

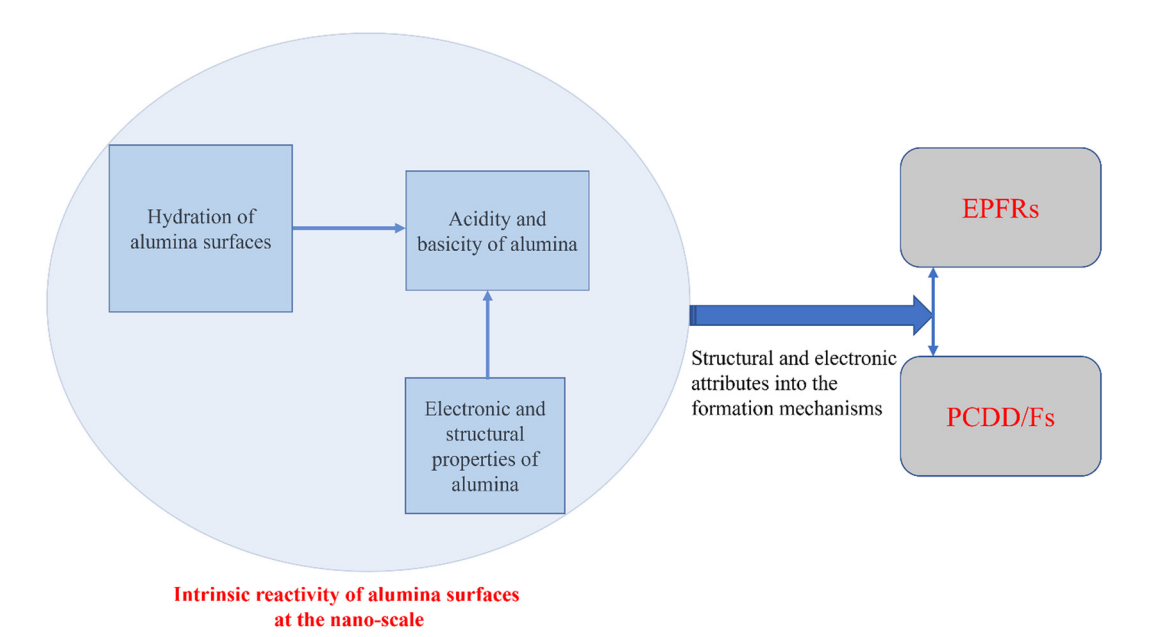
A significant number of experimental and theoretical studies have addressed many aspects related to aluminium-containing compounds, mainly focusing on their structures, electronic properties, stability, and most importantly their applications. Herein, we limit this survey to the chemical reactivity of the surface with an emphasis on the effect of the degree of hydration and acidity. The structure of alumina oxide is discussed to shed light on its relations with the experimentally observed catalysing effects.

The aim of this contribution is thus to critically discuss the acidity and basicity of alumina; a surface attribute that largely dictates its environmental catalytic capacity; the reactivity of alumina towards water molecules (*i.e.* hydration reactions); to evaluate the effect of surface hydration on the catalytic activity of alumina; and most importantly, to survey the well-documented role of alumina oxide in mediating the formation of notorious polychlorinated dibenzo-p-dioxin and polychlorinated dibenzofurans (PCCD/Fs). The survey thoroughly presents and illustrates pertinent literature findings to the nano-based effect of alumina surfaces in forming a wide array of pollutants. The intent herein is not to provide a comprehensive account of the role of alumina as catalyst supports but rather of their role as

important surface mediators in the formation of EPFRs. This review is organised as follows: the first few sections present the structural and electronic properties of alumina, followed by surveying hydration reactions of alumina before presenting an overview of the formation of PCDD/Fs and EPFR and the underlying role of alumina. In this review, we focus only on the most thermodynamically stable form of alumina, α -Al₂O₃ (corundum) [10]. Hydration reactions of alumina are briefly surveyed herein as they are directly related to the acidic and basic sites in alumina; the latter underpin the catalytic reactivity of alumina. The role of alumina in the surface-mediating formation of EPFRs and halogenated dioxins, in general, stems from structural and electronic features, computed or measured at the nano-scale. For this reason, this review devotes the opening section to cover these aspects. Scheme 1 presents a road map of the review.

2 Crystal structure and electronic properties of bulk α -Al₂O₃

The crystal structure of α -Al₂O₃ belongs to the $R\overline{3}c$ space group, with either the trigonal unit cell, that is, hexagonal coordinated with six formula units consisting of 30 atoms in total, and/or the rhombohedral unit cell consisting of two molecular units (*i.e.* 10 atoms) [11]. The α -Al₂O₃ unit cell displays a close-packed ABAB alternating sequence stack of oxygen ions and Al ions, which occupies



Scheme 1: An overview of the survey.

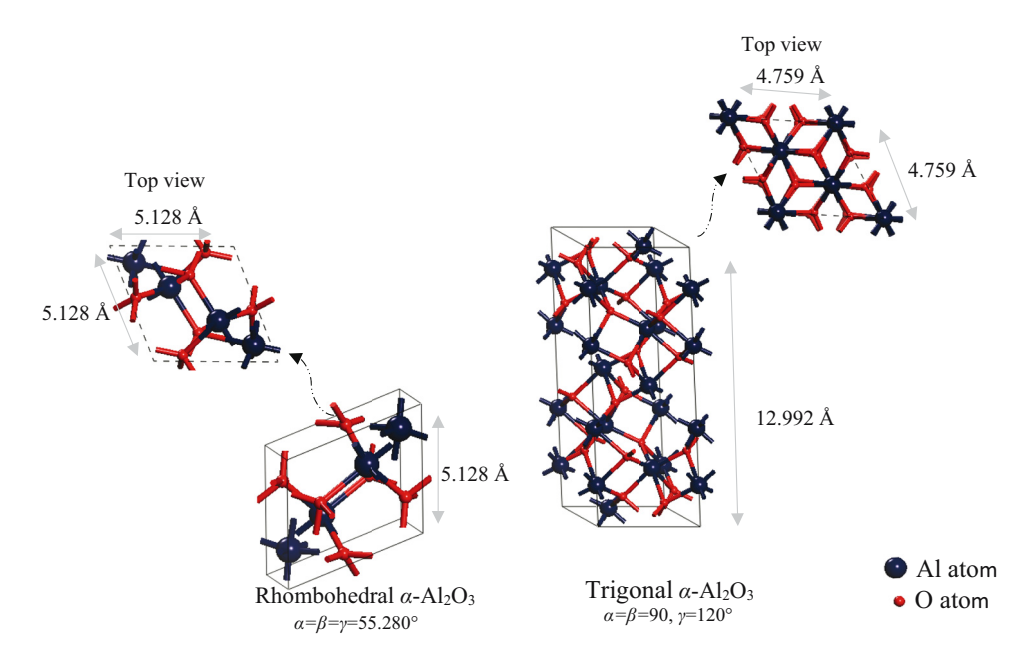


Figure 1: Crystallographic classification of both trigonal and rhombohedral unit cells of α-Al₂O₃.

two-thirds of the six-fold coordinated sites between the oxygen layers [12]. Figure 1 shows the crystallographic classifications of both the trigonal and rhombohedral unit cells of α -Al₂O_{3.}

Figure 2 illustrates our computed electronic band structure and the total density of states (DOS) of bulk α -Al₂O₃. The location of the bands is highlighted in Figure 2. The system represents a wide insulating gap of 6.31 eV, which is consistent with other theoretically calculated values stated for α -Al₂O₃, namely 6.26 [13]

and 6.32 eV [11]. The band gap serves as the energy difference between the highest occupied molecular orbitals (HMO) and the lowest unoccupied molecular orbitals (LUMO). A notable difference between the upper valence band (UVB) and the conduction band (CB) was observed by Mousavi *et al.* [11]. Unlike the flat behaviour of the electron states at the top of the VB, CB displays a large curvature, indicating a large effective whole mass of the VB, as well as good mobility for electrons at the CB [11].

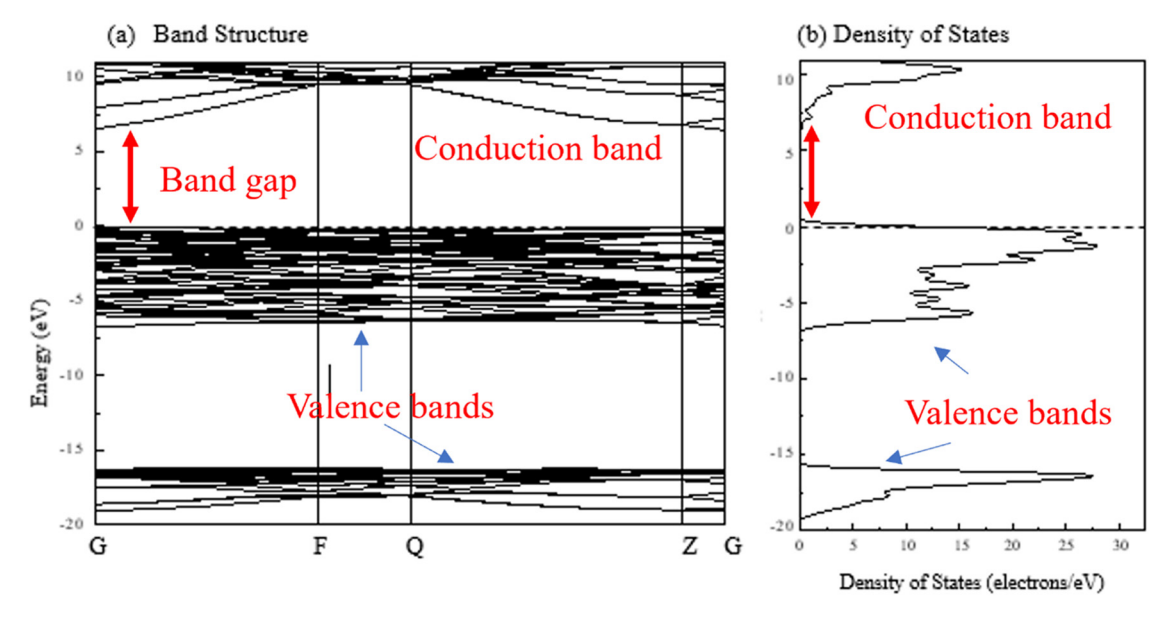


Figure 2: Electronic properties of bulk α -Al₂O₃: (a) electronic band structure and (b) total DOS.

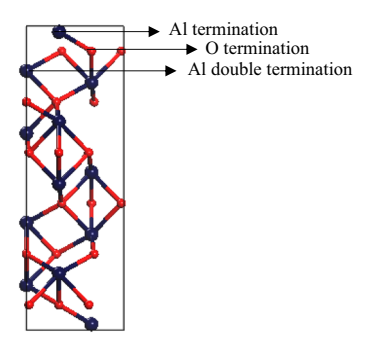


Figure 3: α -Al₂O₃ hexagonal unit cell. The terminations labelled Al, O, and Al double can serve as ideal terminations for the 0001 surface (*i.e.*, a bulk-like termination).

The calculated DOS contains two valence bands: UVB and the lower valence band (LVB). The LVB extends from 19.9 to $-15.2\,\mathrm{eV}$ and mainly consists of two peaks located at approximately -17.6 and $-16.4\,\mathrm{eV}$, while the UVB extends from -7.5 to $0.91\,\mathrm{eV}$. The UVB consists of many peaks that act as a source of electrons contributing to the transition to the CB [11]. The calculated ionic band gap (the gap between UVB and LVB) was found to be $7.7\,\mathrm{eV}$, which is consistent with the reported results by Perevalov *et al.* [13] of $8.9\,\mathrm{eV}$. Clearly, such a band gap confirms the iconicity of bulk α -Al $_2$ O $_3$ (*i.e.* +1.092e and -0.702e are the reported atomic Mulliken charges for Al and O atoms, respectively [14]).

3 Structural aspects of the α -Al₂O₃ (0001) surface

The structure of a bulk hexagonal unit cell of α -Al₂O₃ affords different non-equivalent low-index plane orientations. Of these orientations, the α -Al₂O₃ (0001) surface is the most thermodynamically stable configuration [15]. The (0001) surface of α -Al₂O₃ has been the subject of numerous experimental [16–21] and theoretical [22–29] investigations since it is widely used as a substrate in many catalytic-based applications. The (0001) surface of α -Al₂O₃ (shown in Figure 3) displays three distinct atomic terminations on the surface: Al termination with an Al surface layer followed by an O layer; O termination with an oxygen surface layer followed by an Al layer; and Al double termination with an Al surface layer followed by an Al layer (refer to Figure 3).

Several investigations [18,19,30,31] on α -Al₂O₃ demonstrated Al termination to be the most energetically stable. Tasker [30] attributed this stability from electrostatic and electronic considerations to the non-polarity of

this termination. Unlike the other terminations, the net dipole moment of Al termination, resulting from the stacking Al–O–Al, stands at zero. Other analogous studies [26,28,29] attribute the profound stability of the three terminations to the stoichiometry at the surface, which depends on the alumina/oxygen chemical potential. For instance, the Al-terminated surface assumes a bulk-like termination. Therefore, its energy is independent of the Al and/or O operating chemical potential.

Early research on α -Al₂O₃ focused on estimating the relaxation of the (0001)-Al terminated surface. Theoretical calculations of Manassidis *et al.* [32], using the density functional theory (DFT) within the local density approximation (LDA) framework, predicted that the surface displays a significant inward relaxation, which involves a downward displacement of the Al layer (*i.e.* the first layer) towards the O layer (*i.e.* the second layer) of 85% relative to the bulk. These results were later confirmed through a similar theoretical approach by Kruse *et al.* [33]. The large surface relaxation was also confirmed by Verdozzi *et al.*, who obtained a very similar relaxation of 87% [27]. However, X-ray diffraction [27] and ion-scattering [18] experiments conclude a relaxation of 35%, which is significantly lower than the value predicted by theoretical modelling.

The debate regarding the interpretations of the large inward relaxation of the surface Al layer has been expanded with the argument that the large relaxation behaviour of the surface is related to the formation of an sp² bond between the Al and O surface atoms [34]. Batyrev *et al.* [25] stated that the large relaxation is unlikely to be related to the formation of sp² because there is no evidence of sp² bonding in any of the experimental and theoretical studies. However, the authors attribute this strong relaxation to the electrostatic force.

4 Acidity and basicity of alumina

The α -Al₂O₃ (0001) surface consists of co-ordinately unsaturated sites. Accordingly, the surface is easily covered by different types of adsorbed species. The difference in the coordination number of Al³⁺ surface atoms (*i.e.* tetrahedral and/or octahedral) leads to the formation of a variety of chemical sites on the alumina surface, which has a pivotal role in chemical processes [35]. Furthermore, the ratio of the Al³⁺ ion, including both coordination sites and the oxygen lattice density, can result in various transition aluminas, making the surface chemistry of alumina a highly complex subject [36]. Water, as an abundant component, constitutes the most commonly adsorbed species.

Depending on the temperature and pressure, water adsorbs on the surfaces either physically (*i.e.* non-dissociated) *via* hydrogen bonding and/or chemically (*i.e.* dissociated) forming surface hydroxyl groups [37].

Water dissociation over the alumina surface leads to the formation of a surface hydroxyl group [37,38], starting from the physisorbed (non-dissociated) interaction at room temperature. With the increase in temperature, water gradually desorbs from the surface changing the chemistry of the surface significantly [38-40]. The extent of the dehydration of alumina assumes a significant role in controlling the surface acid-base properties. For instance, desorbing one water molecule from two adjacent hydroxyl groups causes the formation of a strained oxygen bridge, followed by the appearance of active Lewis acid-base sites [41]. However, this change does not terminate at this point. When an alumina surface co-exists with a sufficient amount of water, the surface Lewis acid sites are converted into (very weak) Brønsted acid sites, arising from the basic properties of the surface. Figure 4 illustrates a simple schematic of the generation of acidic-basic sites and Brønsted acid sites over the alumina surface [41,42]. The Al⁵⁺ originates from a five-coordinated arrangement. Such unique coordination has been recently confirmed by accurate ultra-highfield solid-state NMR [43].

Both Lewis acid-base sites, which are generally generated after dehydration/dehydroxylation [44–50], have been thought of as a key factor in deriving the catalytic activity of alumina surfaces [41]. It is generally viewed that Brønsted acid sites facilitate dehydration reactions (*i.e.* water elimination), while Lewis acid and basic sites mediate surface hydrogenation [51]. As stated above, the dissociation of water molecules over exposed Al cations forms adsorbed hydroxyl surface groups, OH^{ads}. Dissociated hydrogen atoms form other surface OH groups,

OH^{sur}. The latter signify the Brønsted acid sites that can coordinate with other species, whereas Lewis acid sites can exchange their OH^{ads} groups [52]. The absolute atomic charge held by each site depends on the coordination number of both the OH groups and the nearby Al sites. For singly coordinated OH groups, surface Al sites are connected to five bulk oxygen atoms in addition to a hydroxyl group. As such, Al cations donate 1/2 charge unit to each oxygen atom in the hydroxyl groups Al₁-OH^{-0.5}. This renders Al as basic sites. For doubly coordinated OH sites, the oxygen atoms receive 1/2 charge unit from each of the Al cations. This renders the net charge at the oxygen atoms to be zero, i.e. Al₂–OH^{0.0}. In the triply coordinated hydroxyl groups, oxygen atoms accept a 1/2 charge unit from Al sites, and thus, they entail a net positive charge of 0.5, i.e. Al₃-OH^{+0.5}.

Different models of surface hydroxyl groups have been suggested to elucidate the reactivity of alumina surfaces [37]. Table 1 summarises the types of hydroxyl groups based on these models and their associated vibrational frequencies, while Figure 5 portrays the types of bondings according to these models. The early Peri's model [40] is unable to encompass the entire hydroxyl group of transition aluminas as it assumes that (100) is the only plausible termination of alumina. This was corrected by the model of Tsyganenko and Filimonov [53], which considers all other surface terminations. A more comprehensive model was suggested by Morterra et al. [37] that treats the coordination of the surface cation (i.e. Al) as a key factor in determining the surface hydroxyl group frequencies. Finally, Knozinger's model suffers from the limitation that there is no surface reconstruction and/or ion migration, even at high temperatures [54]. Finally, Busca's model [55] incorporated the role of surface cation vacancies and the coordination of the cation.

Figure 4: Formation of Lewis acid-base sites over the alumina surface [41,42].

Table 1: Types of hydroxyl groups on alumina and their associated frequencies

OH bond	Frequency (cm ⁻¹)	Peri's model [40]	Tsyganenko's model [53,56]	Knozinger's model [57]
1	3,800	A	1	lb
2	3,775	D	1	la
3	3,745	В	II	IIb
4	3,730	E	II	lla
5	3,710	C	III	Ш
6	3,690	C	III	Ш
7	3,590	H-bonded		H-bonded

The coordination by each group is described in three models as shown in Figure 5. For example, the vibration associated with category III according to Tsyganenko's classification is equal to $3,710\,\mathrm{cm}^{-1}$

Chemical sites over alumina surfaces have been detected experimentally either directly by the O–H stretch using

infrared (IR) spectroscopy [40,58] (i.e. BrØnsted acid sites, Al-OH) and/or indirectly by the adsorption of IR-absorbing probe molecules (i.e. Lewis acid-base sites, Al^{3+} and O^{2-}) [54,59]. The change in the IR spectra from the neat alumina surfaces upon interaction with a species indicates the occurrence of a chemisorption or a physisorption process. As will be discussed in the following sections, catalysis by alumina surfaces stems from their facile capacity to undergo dehydration and dihydroxylation reactions. For instance, the desorption of a water molecule from the surface affords one Al³⁺ cation and one O²⁻ anion. Thus, this reaction creates active Lewis acid-base sites. As such, the process of dihydroxylation correlates with the description of alumina surfaces based on Tsyganenko's [53] and Knozinger's [54] models, whereas nearby OH groups desorb at lower temperatures and isolated groups desorb at higher temperatures. In a nutshell, catalysis by alumina is governed by its acidic and basic sites.

Apart from previous models, several investigations [35,40,58] deployed the IR spectroscopy observations to classify surface hydroxyl groups into two main groups:

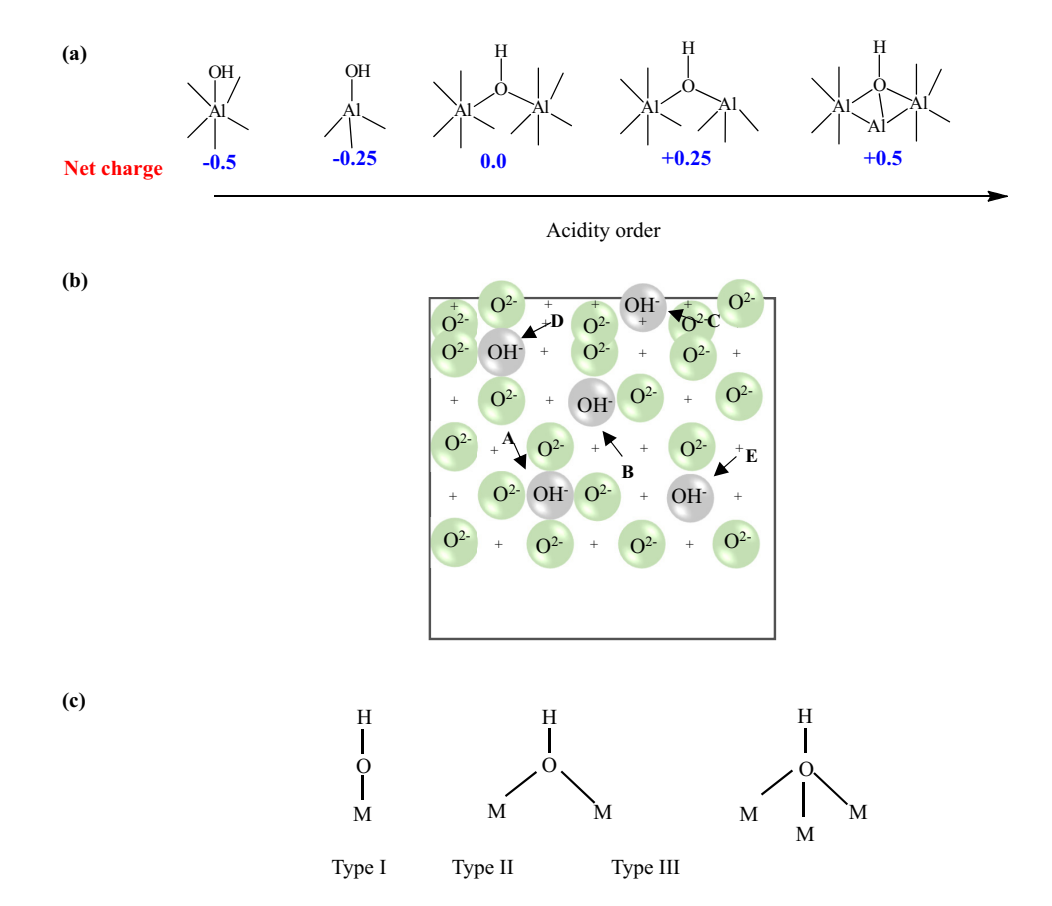


Figure 5: (a) Categories of hydroxyl groups and coordination numbers of Al cations according to the Knozinger model [54]. (b) The Peri model representing five different types of surface hydroxyl groups ("+" represents Al³⁺ of the lower layer) [42]. (c) Surface hydroxyl groups based on Tsyganenko's classification [53,56]. The symbols A–E in (b) refer to the category of the OH group as described in Table 1 by Peri's model.

isolated hydroxyl groups with sharp IR bands (>3,600 cm⁻¹) and self-associated hydroxyl groups with broad intense bands (<3,600 cm⁻¹). Furthermore, self-associated hydroxyl groups differ from isolated ones in the presence of the hydrogen bond connection between each group. The isolated hydroxyl group has been classified, based on Knozinger's model, into five different types. Figure 6 displays a schematic diagram including both types of hydroxyl groups and their frequencies.

5 Water interaction with alumina surfaces

5.1 A mechanistic overview

As a prominent stand-alone and support of catalysts deployed in many chemical reactions, the hydration of alumina has received considerable critical attention because it affects the chemistry of the surface (reactivity, polarity, and catalytic performance). It has been investigated using various surface science techniques with the underlying aim to elucidate mechanistic pathways that prevail at the nano-scale. All of these proved that the interaction occurs *via* acid-base interactions [60]. The adsorption of water on alumina surfaces principally involves chemisorption, quasi-chemisorption, physisorption, and capillary condensation, which translate into a more profound interactional complexity [61].

In an experimental study using the NMR technique, Rui *et al.* [62] investigated the interaction of alumina and water molecules. They showed that through chemical shift changes (δ_H) and spin-lattice relaxation (T_1), water exists over the alumina surface in three different states:

bound water, pore water, and bulk water. Adsorbed water constitutes hydrogen atoms bonded with the alumina surface and accordingly, it entails the highest chemical shift value and the shortest relaxation time. Conversely, bulk water has the lowest chemical shift value and the longest relaxation time. The authors also found an inverse correlation between the chemical shift value of the adsorbed water and the temperature, which has been attributed to the effect of the temperature on the speed of the molecular motion. As the temperature increases, the gained molecular speed increases the tendency of the bound water to leave the surface: this process led to a decrease in the average chemical shift. Several studies investigated the state of the adsorbed water on alumina surfaces [63]. Likewise, Coustet and Jupille [64], via resolution electron energy loss spectroscopy, demonstrated that water adsorption over alumina mainly occurs by dissociative adsorption. This was also confirmed by the temperature programmed desorption (TPD) study carried out by Elam et al. [65].

A large and growing body of experimental and theoretical literature has investigated the interaction of the α -Al₂O₃ (0001) surface with water molecules, all of which prove that the α -Al₂O₃ (0001) surface is highly reactive towards water molecules in producing surface hydroxyl groups [23,65–74].

A variety of experimental techniques, such as photoemission,[67] thermal desorption [65], calorimetric [23,66], and vibrational spectroscopy [71,72], have indicated that the amount of water exposed to the surface is a principal determining factor of the hydrolysis process. For instance, at low water exposure, hydroxylation of the surface occurs through the active defect sites, whereas a high volume of water exposed to the surface results in the breaking of the Al–O surface bond, and accordingly, hydroxylation of the basal plane.

DFT investigations [68,69,75–77] have confirmed the analogous experimental findings. These studies described

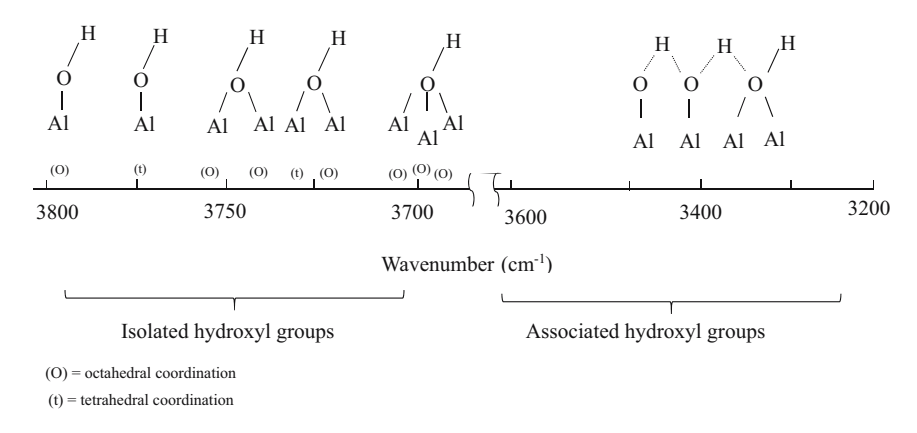


Figure 6: Frequency of hydroxyl group over the alumina surface [35].

Figure 7: Hydrolysis process of the α -Al₂O₃ (0001) surface [74].

in detail the steps of the basal plane hydroxylation, which starts by breaking one of the three equivalent Al_s-O_s surface bonds. Following the fission of multiple surface Al_s-O_s bonds, fully hydroxylated (0001) or gibbsite-like alumina is formed as depicted in Figure 7.

Hass *et al.* [68,69] reported that the initial dissociation steps (*i.e.* at low water exposure) are facile and thermodynamically favoured. They even occur at ambient temperature with trivial activation energy. In a follow-up study, Ranea *et al.* [74] used plane-wave DFT to determine that the following steps (*i.e.* at higher water exposure) proceed along more complex reaction coordinates and occur with higher activation energy than that of the opening step. The authors also confirmed that the hydrolysis of the α -Al₂O₃ surface is governed by the

degree of water coverage. It was illustrated that a significant contribution of intermolecular interactions offsets the effect induced by adsorbate-surface binding at increasing coverage.

It has been shown that water adsorption over the α -Al₂O₃ (0001) surface produces three different states, as shown in Figure 8.

A 1–2 dissociative pathway (when a water molecule dissociates on the same Al–O surface bond) is the most kinetically feasible mechanism, where the Al surface atoms are hydroxylated and the nearby oxygen atoms are protonated. This is followed by a 1–4 dissociation pathway, where water dissociates over two different Al–O bonds. The calculated binding energies for the three states, as reported by Hass *et al.* [68] in their *ab initio* molecular dynamic

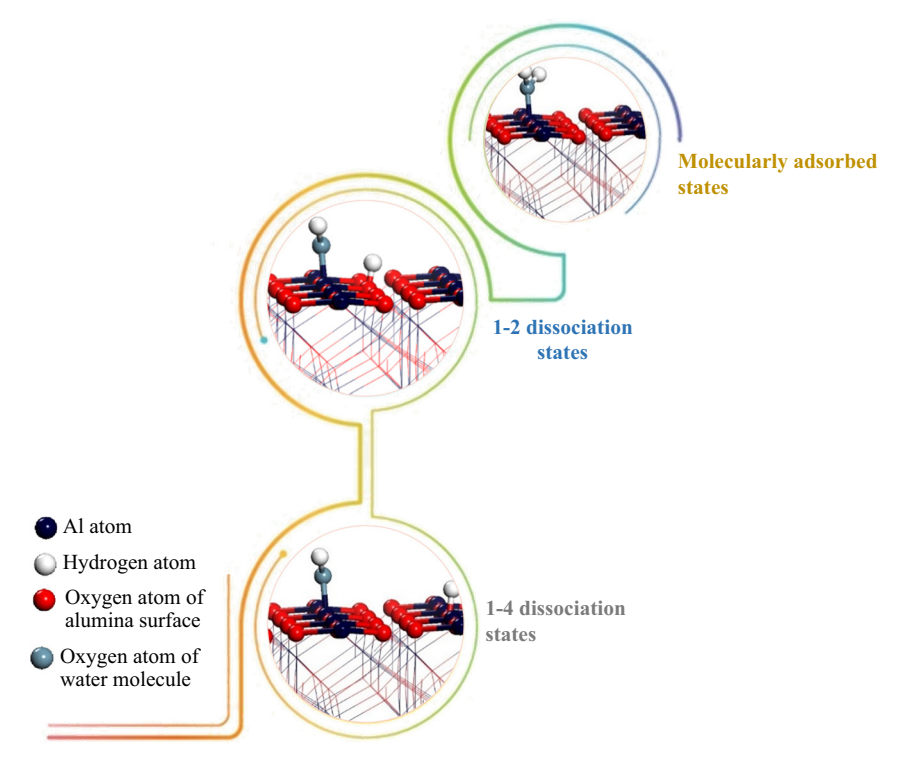


Figure 8: Water over the α -Al₂O₃ (0001) surface.

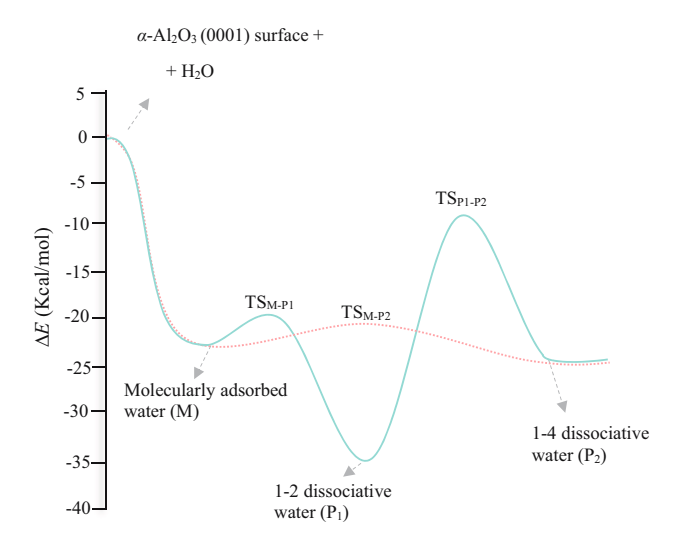


Figure 9: Hydrolysis process of the α -Al $_2$ O $_3$ (0001) surface [14]; TS, transition structure.

study, were predicted to be 97, 139, and 135 kJ/mol, respectively. Wittbrodt *et al.* [75] employed *ab initio* computations to investigate the interaction of water molecules with the Al_8O_{12} cluster, mimicking the extended α - Al_2O_3 (0001) surface. The authors found that dissociation occurs rapidly over the surface (*i.e.* 10^{-2} s) after the water has been physically (*i.e.* molecularly) adsorbed. Figure 9 presents a potential energy surface for H_2O dissociation on the α - Al_2O_3 (0001) surface.

Gaigeot *et al.* [78] used DFT-based molecular dynamics simulation (DFT-MD) to perform a detailed investigation of the behaviour of the (0001) α -Al₂O₃/water interface as an important aspect in determining the interfacial properties, such as acid–base behaviour, dissolution rate, and surface charge. The authors [78] provide an accurate description of the interfacial hydrogen bonding and electron polarisation effects. In addition, based on interfacial hydrogen bonding, they classified the surface hydroxyl groups into two sites: (i) strong and short H-bonding donors and (ii) weak and long H-bonding acceptors. Alternately, one is in the surface

plane and the other is pointing out from the surface, as seen in Figure 10.

The calculated average charges on the O and H atoms of the hydroxyl group were found to be -0.84 and 0.28e, respectively, which is the key electronic descriptor dictating the strength and weakness of both sites [78]. The authors also found that both the H-bonding acceptor and H-bonding donor sites lead to the formation of two species of water molecular interfaces, namely, liquid-like interface and ice-like interface, respectively. Previous studies [72,78-82] provide further information on the vibrational spectroscopy of these two interfaces. Two different spectrum broadbands have been detected, 3,200 and 3,400 cm⁻¹ peak, which are referred to as ice-like interface and liquid-like interface, respectively. Furthermore, the structure of the water/alumina interface was found to be greatly affected by the change in the pH of the reaction medium [81-83].

The catalytic properties (i.e. activity and selectivity) of the alumina surface are directly correlated with the chemistry of the surface where the hydrolysis process assumes a critical role. Evidence suggests that heating and cooling processes are among the most important factors where the degree of hydration coverage (i.e. acidity and basicity of the surface) is highly sensitive to temperature [84]. Based on the results of the IR and NMR measurements, heating and cooling processes can either reversibly add or remove hydroxyl groups on the surfaces [85]. Furthermore, it has been observed experimentally, in a microcalorimetry study conducted by McHale et al. [66], that the degree of hydration over the α -Al₂O₃ (0001) surface is mainly associated with the drying temperature, in which heating at a temperature of >1,000 K dehydrates the surface to almost <9 OH/nm², whereas at a lower temperature of 600 K, the extent of surface hydroxyl group coverage stands at 15 OH/nm². Using X-ray photoelectron spectroscopy (XPS) [67], TPD, and laser-induced thermal desorption (LITD) measurements [65], it was found that the formation of the surface hydroxyl group

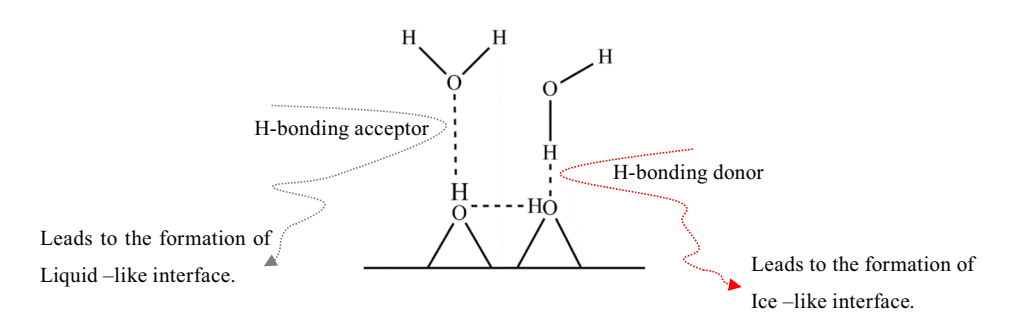


Figure 10: Hydrogen bonding network in the (0001) α -Al₂O₃/water interface [78].

over (0001) α -Al₂O₃ is observed at a temperature as low as 300 K.

In LITD and TPD study of alumina hydration, Nelson *et al.* [86] investigated the desorption of water from the α -Al₂O₃ (0001) surface. They showed that the water desorption process takes place over a wide range of temperatures (*i.e.* 300–500 K), concluding that the alumina surface includes different surface hydroxyl groups with different binding energies ranging from 96 to 172 kJ/mol. A seminal study in this area is the work of Hendriksen *et al.* [87]. The authors demonstrated that molecular water is more readily removable compared to surface hydroxyl groups, in which the latter remains on the surface even at 1,273 K.

5.2 Effect of surface hydration on the catalytic activity of alumina

It has become evident that [38–41,88] the chemical makeup (*i.e.* adsorption and decomposition) of the hydroxyl groups over the alumina surface constitutes a key factor in clarifying the reactive/catalytic nature of alumina [65,69,70]. However, the relationship between the reactivity, surface structure, and degree of hydration remains open to debate [83].

An experimental study by Ballinger and Yates [89] on the behaviour of alumina at high temperatures revealed that dehydration of alumina occurs in the temperature range of 475–1,200 K. The authors also observed a linear correlation between the decreasing integrated absorbance of the hydroxyl group with the increasing integrated absorbance of physisorbed Al³⁺–CO. Another experimental study, using Fourier transform (FT) IR spectroscopy, confirmed that the heat of adsorption over alumina surfaces (*i.e.* both α - and γ -alumina powders) depends primarily on the degree of hydration prior to water adsorption.

Data from several sources have identified that the increased reactivity of the surface atoms on the alumina surfaces is associated with lower atomic coordination numbers, whereby the lower the coordination, the higher the surface acidity or basicity. In a study investigating a selective probe for tri-coordinate Al "defect" sites on 110 and 100 terminations of γ - and δ -alumina, Wischert *et al.* [90] reported that the fully dehydrated 110 surface in both transitions displays three different Lewis acid sites: tri-coordinated (Al_{III}), tetra-coordinated (Al_{IVa}), and tetra-coordinated (Al_{IVb}), whereas the fully dehydrated 100 surface encompasses two Al_V sites. The authors theoretically addressed the potential of deploying both the 110 and 100 γ - surfaces as scavengers for the N₂ molecular gas, and they found that N₂ molecules are significantly

stabilised on the strongest Lewis acid site (*i.e.* tri-coordinated (Al $_{\rm III}$), $\Delta E_{\rm ads}$ (N $_2$) = -45 kJ/mol). Along a similar line of inquiry, Joubert *et al.* [91] demonstrated experimentally that the tricoordinate Al $_{\rm III}$ strong Lewis acid sites on the 110 surface are the highly reactive sites in dissociating H–H and C–H bonds of H $_2$ and CH $_4$ molecules, respectively.

In a follow-up study by Wischert et~al.~[92], the effect of surface hydration on the catalytic activity of the γ -Al $_2$ O $_3$ (100) surface towards the CH $_4$ molecule was investigated. The authors found that water assumes an important role in the Lewis acidity of the surface in a process that is controlled mainly by temperature. For instance, water physically interacts with Al $_{\rm IV}$ sites, increasing the basicity of the neighbouring O $_{\rm surf}$ atom without making any changes in the Lewis acidity of Al $_{\rm III}$, which ultimately results in the formation of a highly reactive "frustrated" Al $_{\rm III}$, O Lewis acid–base site, facilitating dissociation of the C–H bond of CH $_4$ through lower activation energies.

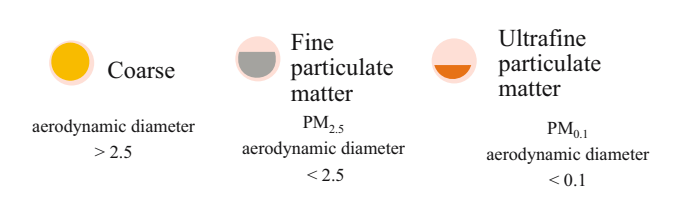
6 Alumina oxide mediated the formation of organic pollutants

6.1 EPFRs

The main sources of air pollution (organic pollutants and particulate matters [PMs]) are typically combustion and thermal processes [93,94]. In the light of size analysis, PMs are often divided into three categories as follows [95–99] (Scheme 2).

Up to 90 and 70% of PM_{0.1} and PM_{2.5}, respectively, are generally produced from combustion processes (*i.e.* internal combustion engines, industrial heating, and biomass burning), which are further categorised as either primary particles (*i.e.* directly emitted particles) or secondary particles (indirectly emitted particles) [100].

EPFRs are a class of toxic compounds when associated with combustion generate airborne fine particles $PM_{2.5}$. They were first demonstrated experimentally by



Scheme 2: Categories of PM in the atmosphere (PM_x stands for the PM where the number (*i.e.*, x) signifies that the average mean diameter is less than $x \mu m$).

11

Dellinger *et al.* [101] in environmental samples collected from different sites, as seen in Figure 11. The same research group later confirmed the presence of the EPFRs in airborne fine particles with a high concentration of 10^1 – 10^{18} radicals/g in samples from Baton Rouge city [102]. In addition to the ambient PM_{2.5}, EPFRs were established on the surface of particles containing active transition metals in the combustion process (*i.e.* post-flame and cool-zone regions) [101,103,104]. The delocalised electron system of EPFR enables them to resist oxidation by atmospheric oxygen. Oxidative stress induced by the EPFR is analogous to that of reactive oxygen species (ROS, such as OH singlet oxygen, and HO₂). Thus, EPFRs can induce serious health problems including chronic respiratory and cardiopulmonary dysfunction [105,106].

Typically, EPFRs are produced from the physiochemical interaction of aromatic hydrocarbons, present in the combustion processes, with the metal oxide powder [104,107,108]. Reliant on the nature of the adsorbate (aromatic hydrocarbons) and the temperature, the different EPFRs produced are generally classified as either semiquinone and/or phenoxyl

types of radicals. Theoretically, it has been demonstrated that the stability of the EPFRs stems from the resonance stabilisation of the phenyl ring. As portrayed in Figure 12, EPFRs encompass both carbon- and oxygen-centred radicals [103,109]. The EPFR formation has been studied experimentally by many researchers using EPR spectroscopy and X-ray absorption spectroscopy (XANES) [103,104,107,108,110–113]. These studies provided a detailed account of the physiochemical interaction of EPFR precursors with selected metal oxide surfaces (*i.e.* Fe₂O₃[107]). They indicated that, in the progressive physisorption and chemisorption processes, the surface metal atoms transfer electrons to the adsorbed organic precursors, successively leading to the generation of persistent surface-bound radicals.

The stability of EPFRs primarily depends on two main factors, namely the nature of the precursor molecule and the metal oxides. Figure 13 contrasts the half-lives of different EPFRs generated over various metal oxides. EPFRs generated from phenol over alumina entail [110] a longer half-life time than most of the investigated transition metal oxides, except that of ZnO.

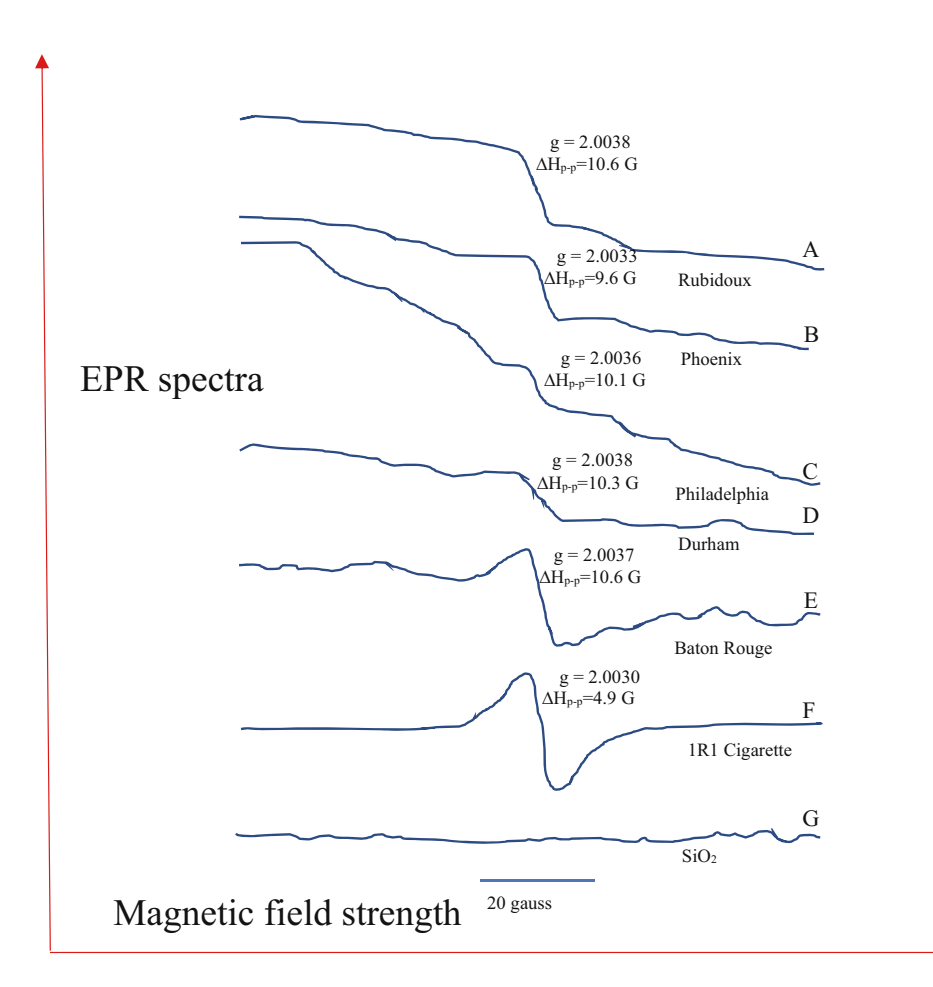


Figure 11: EPR spectra of EPFRs in PM_{2.5} from difference places in the United States [101].

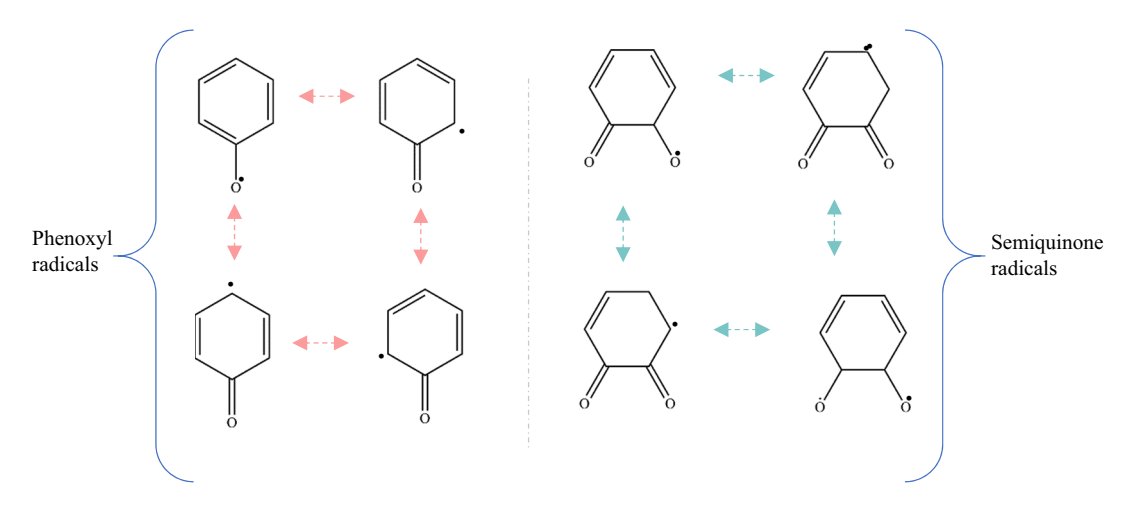


Figure 12: Structural types of EPFRs.

6.2 Role of EPFRs in the heterogeneous formation of PCDD/Fs

EPFRs have been recognised as a key intermediate in the formation of persistent organic pollutants, most notably PCDD/Fs [115–118]. PCDD/Fs are generally formed along two main pathways: (I) high-temperature homogeneous synthesis (gas-phase reactions in the temperature window of 723–973 K) and (II) heterogeneous synthesis (operating in the range of 473–673 K); the latter is divided into two broad channels: precursor synthesis (surface-mediated) and *de novo* synthesis (oxidation of carbonaceous matrix) [119–123].

In the combustion process, high temperatures produce a different type of radicals (*i.e.* semiquinone and phenoxy), which mainly depend on the precursor present and leads to a series of chemical reactions [124,125] and ultimately the formation of PCDD/Fs and other combustion-generated PMs. Figure 14 displays the zone theory of combustion for the formation of PCDD/Fs, which provides an overview of the zones of the combustion processes, including the main pathways and the associated temperature window of each zone. The catalytic formation of PCDD/Fs from the precursor, *via* forming EPFRs, is observed in the last stage of the combustion process,

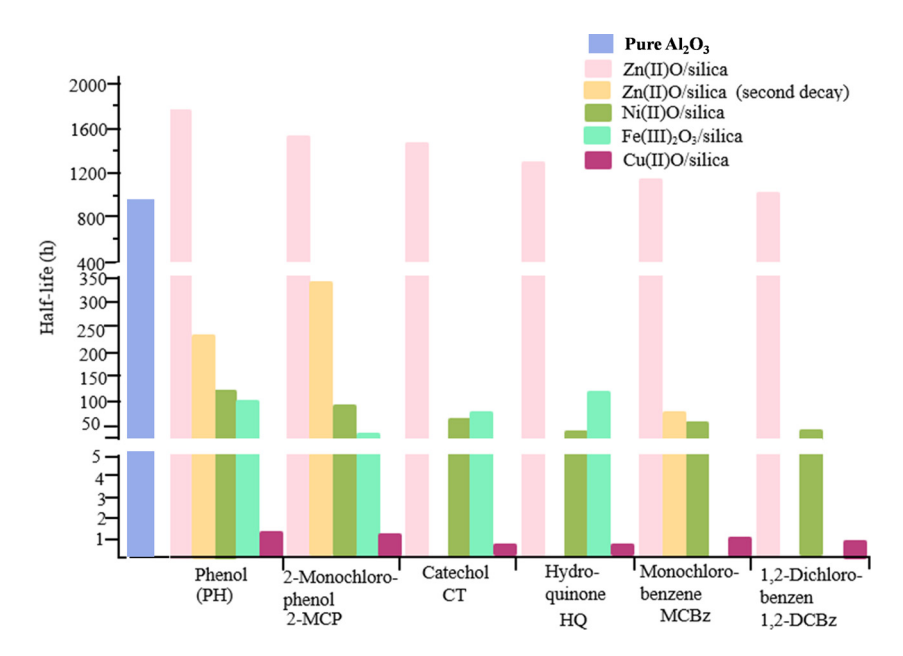


Figure 13: Comparison of several half-lives of different EPFRs generated over different metal oxides [114]. For alumina, data are only available for phenol [110].

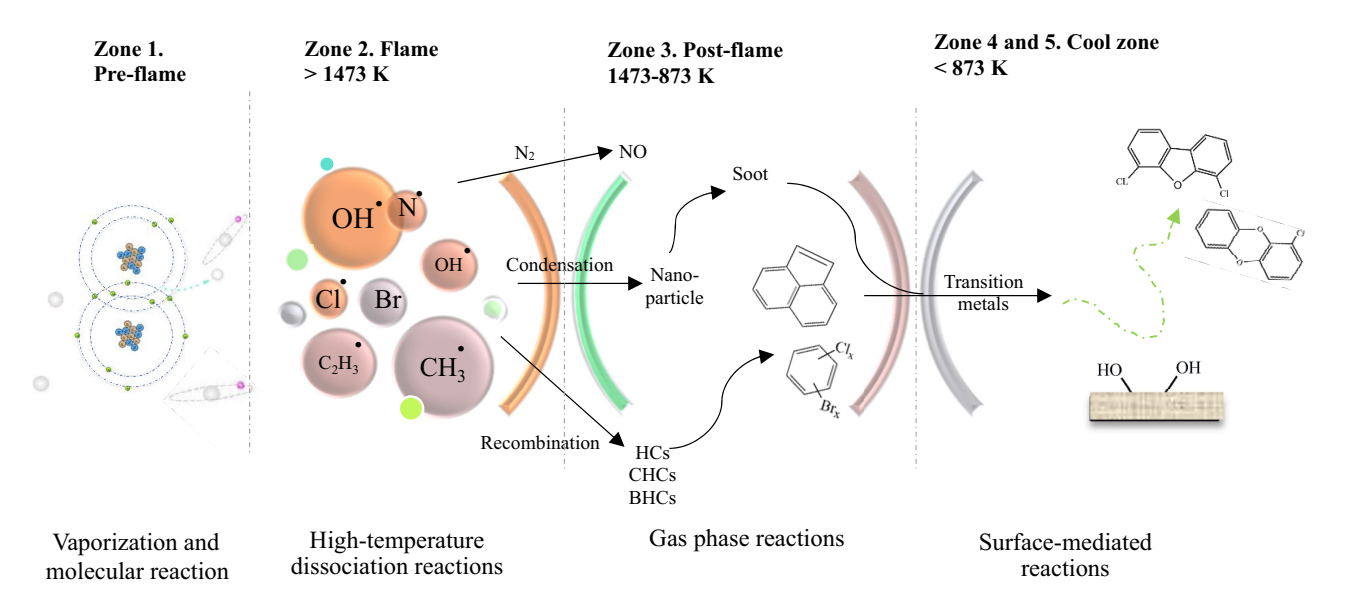


Figure 14: Zone theory of combustion that operates in the formation of PCDD/Fs [102].

particularly, in the cooling zones of the combustion systems (zone 4). In this part of the combustion process, the temperature is typically in the range of 423–873 K. The adsorbed precursor further interacts either with another surface-bound moiety *via* the Langmuir–Hinshelwood mechanism (L–H, depicted in Figure 15) or with a gaseous precursor *via* the Eley–Rideal (E–R, shown in Figure 16) mechanism. The nanoeffect mechanisms presented in Figures 15 and 16 can only be attained through DFT calculations.

6.3 Role of alumina in the formation of EPFRs and PCDD/Fs

Alumina exists as one of the most abundant metal oxides in $PM_{2.5}$ encountered in combustion systems [126–129]. Its concentration in $PM_{2.5}$ can reach 13–16% by mass [6]. Table 2 displays the concentration of alumina and other oxides in fly ash generated from different coal types.

A great deal of research has evidenced that alumina, among the most important transition metals in PM_{2.5}, plays a crucial role in the formation of PCDD/Fs. For instance, Patterson et al. [110] used electron energy loss spectrometry to elucidate the mechanism of EPFR formation over a y-Al₂O₃ surface. The authors report a noticeable shift in π - π * transition of the chemisorbed phenol, suggesting that the appearance of this precursor governs the generation of phenoxy-EPFRs. A recent experimental study by Potter et al. [130] demonstrated the contribution of alumina, α - and y-Al₂O₃, as well as aluminosilicate to the formation of PCDD/Fs from the catalytic oxidation of a 2-monochlorophenol precursor (2-MCP). The authors verified that both alumina and aluminosilicate exhibit an important role in PCDD/F formation. However, the yield of PCDD/Fs mediated by α-Al₂O₃ was only 0.4% (by wt% of the initial reactant). Figure 17 displays the PCDD/F yields from the oxidation of 2-MCP over selected surfaces including both alumina α - and y-Al₂O₃ surfaces. Despite the results of these experiments, a systematic

Figure 15: The L-H mechanism for the formation of PCDFs. A case of a 2-chlorophenol molecule on alumina surfaces.

Figure 16: The E-R for the formation of PCDDs. A case of a 2-chlorophenol molecule on alumina surfaces.

Table 2: Concentration of selected oxides in fly ash generated from different coal types [6]

Component (wt%)	Bituminous	Sub-bituminous	Lignite
SiO ₂	20-60	40-60	15-45
Al_2O_3	5-35	20-30	10-25
Fe_2O_3	10-40	4-10	4-15
CaO	1–12	5-30	15-404
MgO	0-5	1-6	3-10
SO ₃	0-4	0-2	0-10
Na ₂ O	0-4	0-2	0-6
K ₂ O	0-3	0-4	0-4
LOI	0-15	0-3	0-5

mechanistic understanding of how alumina facilitates the formation of EPFR is still lacking.

A series of experimental studies have examined the role of other metal oxides on the formation and persistency of EPFRs in particulates. For instance, Lomnicki et al. [104] and Vejerano et al. [107] investigated the catalytic activity of two transition metal oxides, Fe₂O₃ and CuO, deposited on silicon oxide surfaces. They investigated the catalytic activity of both oxides towards five different aromatic hydrocarbons, namely phenol, hydroquinone, 2-monochlorophenol, 1,2-dichlorobenzen, and catechol. They confirmed that both the Fe₂O₃ and CuO surfaces mediate the formation of EPFR species (both phenoxy and semiquinone types of radicals). They also describe in detail the surfacemediated process, starting from the physisorbed interaction of the precursors, followed by its dissociation states, and ending with the EPFR formation. Furthermore, the authors indicated that surface metal atoms transfer electrons to the bound precursors resulting in the synthesis of EPFR. Some studies have also been carried out to investigate the influence of Ni₂O [108], ZnO [114], and TiO₂ [113] on the formation of EPFR, demonstrating their importance in EPFR formation.

Theoretically, Pan *et al.* [131] investigated the formation of EPFR generated from 2-chlorophenol (2-CP) over hydrated and dehydrated silica surfaces using DFT.

The authors demonstrated that the dehydrated silica cluster is more active towards the attack of 2-CP if contrasted with hydrated configurations. Results from the study unequivocally point out the role of surface acidity in the formation of EPFRs. However, an intriguing question arises if the same trend applies to alumina and other metal oxides. Along a similar line of inquiry, Mosallanjad et al. [115] conducted a study to investigate the formation of PCDD/Fs from neat silica-mediated 2-chlorophenol, confirming the catalytic role of silica surfaces in the generation of PCDD/Fs. The authors attempted to evaluate the impact of temperature on the surface catalytic activity of silica by applying the process in two temperature ranges (523-673 and 823-973 K), representing the lower and the upper range, respectively, of the catalytic regime of PCDD/F formation. They confirmed that the catalytic pathway over neat silica was observed only in the upper range. However, the authors also recognised the critical role played by the fly ash matrix in the PCDD/F formation, even in the absence of transition metals (i.e. neat silica, neat alumina, and alumina-supported iron oxide [132]).

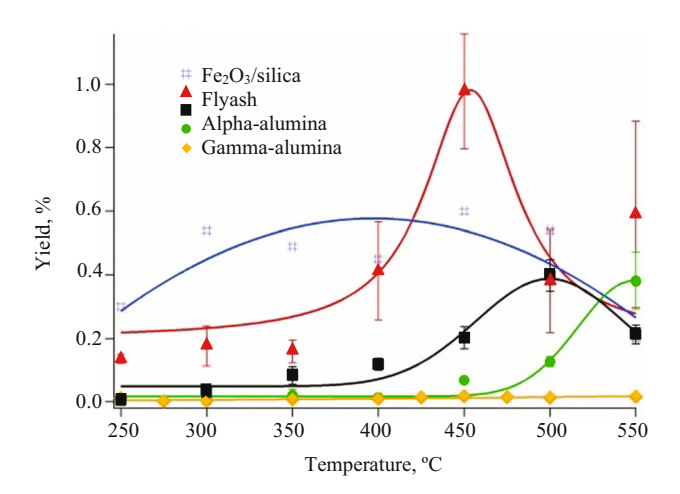


Figure 17: PCDD/F yields from the oxidation of 2-MCP over selected surfaces [130].

DE GRUYTER Formation of EPFRs on alumina — 15

6.4 Alumina surfaces mediated the formation of EPFRs

The interaction of phenol with y-alumina resulted in a paramagnetic signal that is commonly observed over other transition metal oxides, with distinct characteristics. For instance, the paramagnetic signal for the adsorption of phenol over y-alumina entails a g-value of 2.0043 and a peak width of 9.6 G. The observed broadness of the peak indicated a possible co-existence of several EPFR species [110]. When compared with TiO₂, the observed peak featured a g-value of 2.0032. The latter value indicates an electron located at an ortho position of the phenoxy O. The combination of several peaks in the case of alumina interaction with phenol most likely originates from the adsorption at different acidic sites according to the alumina-OH models described in Section 4. Likewise, it was suggested that the presence of various surface terminations assumes a critical role in producing different EPFRs. Radicals bounded to y-alumina surfaces exhibited two decay profiles: one with a 1/e half-life of only 2.5 days while the second one prolonged to a 1/e half-life of 40 days. This was evident through a simultaneous increase in the g-value from 2.0043 to 2.0046 [110]. Such a shift may infer that the remaining radicals on the surface may be phenoxy radicals, or even the more stable semiquinone radicals. The initial g-value was attributed to phenyl radicals adsorbed in a horizontal orientation.

Different transition oxides assume differences in types, concentrations, and mechanisms pertinent to the production of EPFRs. The capacity of alumina to promote the formation of EPFRs exceeds that of other metal oxides. This was attributed to the ease of the oxidation of its Al cations [133]. It was illustrated that the effectiveness towards the

synthesis of EPFRs follows the order Al₂O₃ > ZnO > CuO > NiO. Morphologies were also regarded as an important factor. The seminal work by Liu et al. [133] systematically investigated the formation of EPFRs over various metal oxides, including alumina, starting from 2,4-dichloro-1napthol. The g-factors for radicals obtained over alumina significantly overshoot the corresponding values acquired over other transition metal oxides. This translated in higher concentrations for EPFRs mediated by alumina, as shown in Figure 18a. In particular, alumina selectively promoted the formation of monochlorinated species. As it was the case in the interaction of alumina with phenol, the obtained electroparamagnetic spectra for 2,4-dichloro-1-napthol exhibited an asymmetrical profile indicating the formation of more than one category of EPFRs. Both phenolic and semiquinone-type EPFR radicals were formed. The formation of these distinct EPFRs indicates the occurrence of reaction mechanisms that involve either HCl or H₂O elimination. As shown in Figure 18b, micrometre-sized alumina resulted in the formation of a lower concentration of EPFRs when compared with the regular alumina nanoparticles. The reaction of basic O⁻ sites in alumina's nanoparticles with halogenated pollutants in the atmosphere opens a potent pathway for the formation of EPFRs. This pathway contributes in parallel to the widely suggested direction for the formation of EPFRs from thermal processes.

Along the same line of inquiry, Ye *et al.* [134] investigated the formation of EPFRs over iso-structural metalorganic frameworks (MOFs) where Al, Cr, and Fe constitute the metallic-active ingredients. Initial precursors included chlorinated phenols and catechol. Al³⁺-rich MOF facilitated the formation of EPFRs that endured a half-life of up to 70 days. Insufficient Lewis acidity associated with Cr³⁺ and Fe³⁺ sites significantly hinders the formation of EPFRs

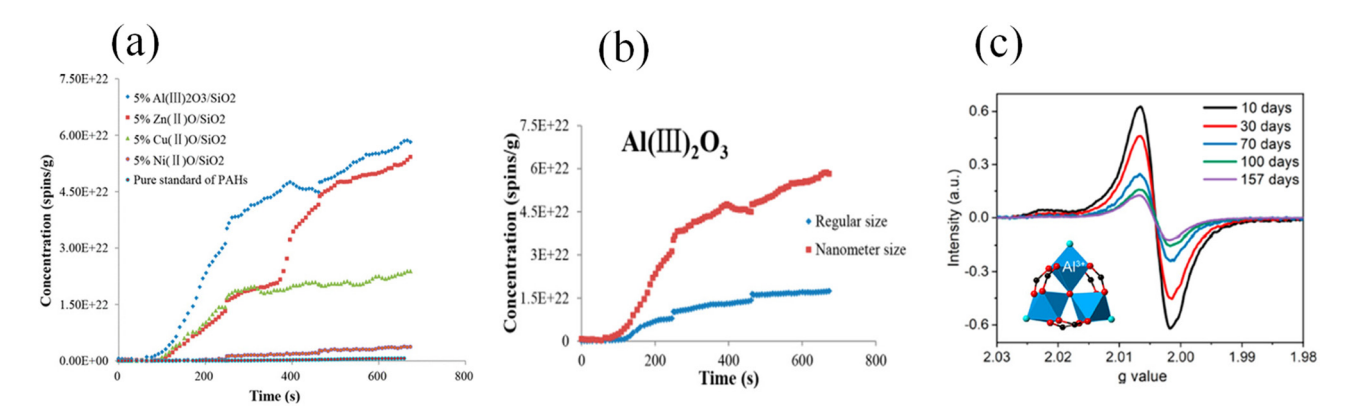


Figure 18: (a) Concentrations of EPFRs over alumina and other transition metal oxides. Reproduced with permission from the American Chemical Society [133]. (b) Effect of alumina morphology on the yield of EPFRs over alumina. Reproduced with permission from the American Chemical Society [133]. (c) The building structure of the Al₂O₃-MOF and the corresponding EPR spectra. Reproduced with permission from the American Chemical Society [132].

Scheme 3: Generic formation mechanisms of EPFRs over alumina.

when contrasted with Al^{3+} sites. For this reason, it was concluded that the synthesis of EPFRs originates from the presence of Lewis acid sites, regardless of the oxidation capacity of the involved metallic species. Deploying magnetic resonance spectroscopy measurements confirmed the unpaired electron donation. Figure 18c shows the building structure of the Al_2O_3 -MOF and the corresponding EPR spectra [134].

Diffused reflectance infrared Fourier transform spectroscopy (DRIFTS) provided insightful mechanistic aspects with a prime focus on the vibrations associated with the temperature-induced departure of water molecules that leads to the emergence of Al3+ sites. Thermal treatment of monochlorophenol and catechol at 250°C afforded strong asymmetrical peaks with g-values of 2.0044 and 2.004, respectively. The absence of hyperfine splitting indicated a weak interaction between Al³⁺ and the unpaired electron of the phenoxy's O of the initial precursor. The observed gvalues reflect the formation of both oxygen- and carboncentred radicals. The interaction of the Al₂O₃-MOF with catechol produced phenolate oxygen-centred radicals, rather than the expected semiquinone-type radicals [134]. The concentrations of EPFRs resulting from monochlorophenol are lower than those observed from catechol. However, in both cases, the synthesis of EPFRs stems from the parent precursors rather than from the secondary decomposition products.

In a related study, Liu *et al.* [135] employed a combined experimental—theoretical approach to investigate the formation of EPFRs over α - and γ -Al₂O₃ starting from pentachlorophenol. It was found that the strong catalytic capacity of both forms of alumina resulted in

the dichlorination of the parent pentachlorophenol. As such, the pentachlorophenoxy radical was not detected. The formation of methyl-substituted phenoxy radicals and long-chain products promotes the authors to assume the role of the dissociated chlorine atoms. More specifically, it was assumed that the alkylation process is facilitated by the conversion of Lewis acid sites into Brønsted acid sites. The lower chlorinated isomers of phenoxy radicals were detected over the two alumina surfaces with *g*-values in the range of 2.0049–2.0055. Steric protection at the *para* position increases the lifetimes of EPFRs over alumina surfaces. This is achieved by avoiding intramolecular reactions from neighbouring adsorbed species [136].

6.5 Mechanistic considerations

6.5.1 General overview

Guided by EPR and DRIFTS measurements, a general mechanistic pathway was proposed for the formation of EPFRs over hydroxylated alumina surfaces [137]. Scheme 3 depicts the general features of this mechanism starting from a 2-chlorophenol molecule as the initial precursor:

The reaction begins with the adsorption of a 2-chlorophenol molecule. As shown in Scheme 2, the terminal OH groups assume a key role in the formation of phenoxy- and semiquinone-type EPFRs. The removal of the phenolic H atom together with a surface OH group (*i.e.* water elimination) results in the formation of a chlorophenolate adduct. The fate of this intermediate is either stabilisation into

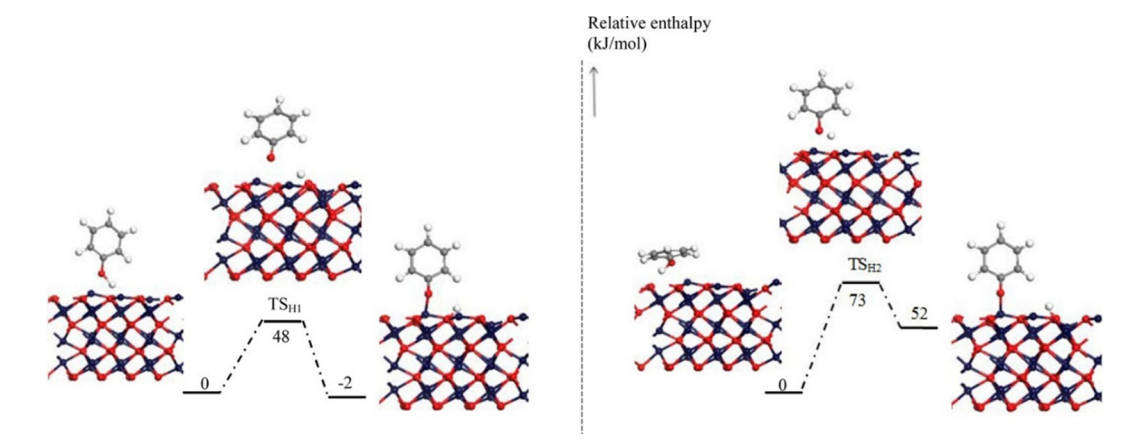


Figure 19: Formation of phenolate over a neat α -Al₂O₃(0001) surface. Reproduced with permission from the American Chemical Society [7].

phenoxy-type EPFRs or to undergo self-coupling into dioxinlike compounds [137]. Water elimination is accompanied by an electron transfer from the aromatic moiety to the Al³⁺ sites; a process that leads to Al reduction. A parallel HCl elimination pathway leads to the formation of semiquinone-type EPFRs. To the best of our knowledge, the literature presents no DFT accounts on the relative importance of these two competing pathways, HCl *versus* water elimination. Thus, it will be insightful to compute corresponding kinetic parameters to assess the relative importance of both routes.

6.5.2 Related DFT studies

In previous DFT studies [7–9], we presented detailed theoretical investigations into the role of alumina oxide-based

models in surface-mediating formation of EPFR, a situation that is typically encountered during the interaction of aromatic compounds with the generated particulate matter PM₁₂ in combustion. We considered different models of alumina, encompassing: dehydrated alumina surfaces, Si-doped alumina surfaces and clusters with different hydration coverages. First, we characterised the catalytic potential of the neat α-Al₂O₃(0001) surface in producing the phenolic-type EPFR, under conditions pertinent to the cooling zones of the combustion system [7]. We found that surface-assisted rupture of the phenol's O-H bond over a dehydrated alumina surface required only 48 kJ/mol to proceed with the manifestation of the facile nature of producing adsorbed phenolate, as shown in Figure 19. Furthermore, the relevance of the acidity sites to the catalytic activity of alumina was clearly supported by the finding that

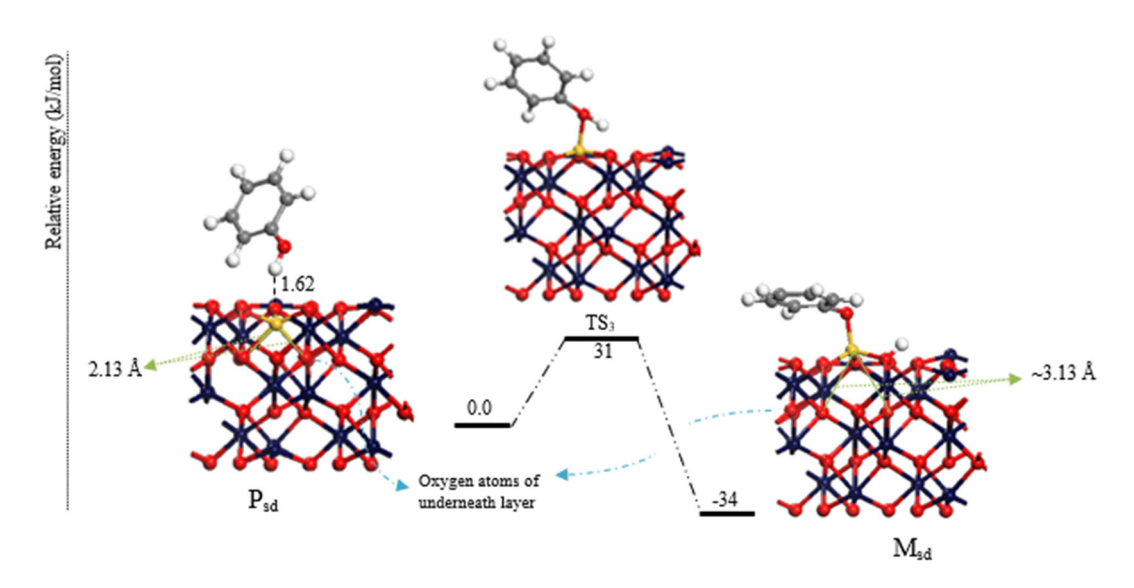


Figure 20: Formation of a phenolate over a Si-doped alumina surface [8].

the catalytic activity of the alumina surface in producing the phenoxy/phenolate species negatively correlates with the degree of hydroxyl coverage.

When considering alumina clusters, we found that clusters with the active Al=O double bond are catalytically more active in mediating the formation of phenolate in reference to structures where all Al-O bonds are saturated (*i.e.* Al-O single bonds) [9]. The Si-doped atom (Figure 20) was found to increase the catalytic activity of the dehydrated alumina surface in producing phenolate adduct, in which the required energy barrier for the formation of phenoxy moiety decreased by 17 kJ/mol compared to the undoped surface (*i.e.* 48 kJ/mol, reported for the pure surface).

Very recently, Wang *et al.* [138] mapped out detailed mechanisms for the formation of phenoxy-type EPFRs from the adsorption of phenol over γ -Al₂O₃ surfaces with different hydration levels. The role of the catalytic effect by ambient water was highlighted in the study. It was illustrated that activation energies required for the surface-mediated fission of the phenolic O–H bonds correlate with the strength of the basic sites. The interaction of phenol with anhydrous alumina at lower water coverages forms phenoxy-bounded EPFRs *via* direct fission of the O–H bonds, whereas at surfaces with high water coverages, the process involves water elimination steps. Figure 21 shows the pertinent mechanism for the latter case.

7 Potential catalytic applications of alumina surfaces

Hydration of alumina surfaces may entail catalytic applications in strategic areas, most notably hydro-deoxygenation (HDO) of biomass fragments. Currently, most HDO reactions take place over non-hydroxylated surfaces such as ceria [139]. Surface hydrogens sourced from the hydroxyl groups may have the potential to initiate surface-assisted hydrogenation reactions with and without inlet streams of hydrogen. Along the same line of enquiry, facile removal of surface hydroxyl groups may afford alumina surfaces an oxidation capacity towards hydrocarbon pollutants. We envisage that these directions present potential catalytic applications of alumina.

8 Perspectives and future outlooks

This review focused on the functionality of alumina surfaces in facilitating the formation of EPFRs. However, despite many experimental studies, reaction mechanisms for the interaction of structurally related precursors with alumina surfaces leading to EPFRs and PCDD/Fs remain largely speculative. Future research is required to address the formation of other types of EPFRs (such as phenyl and

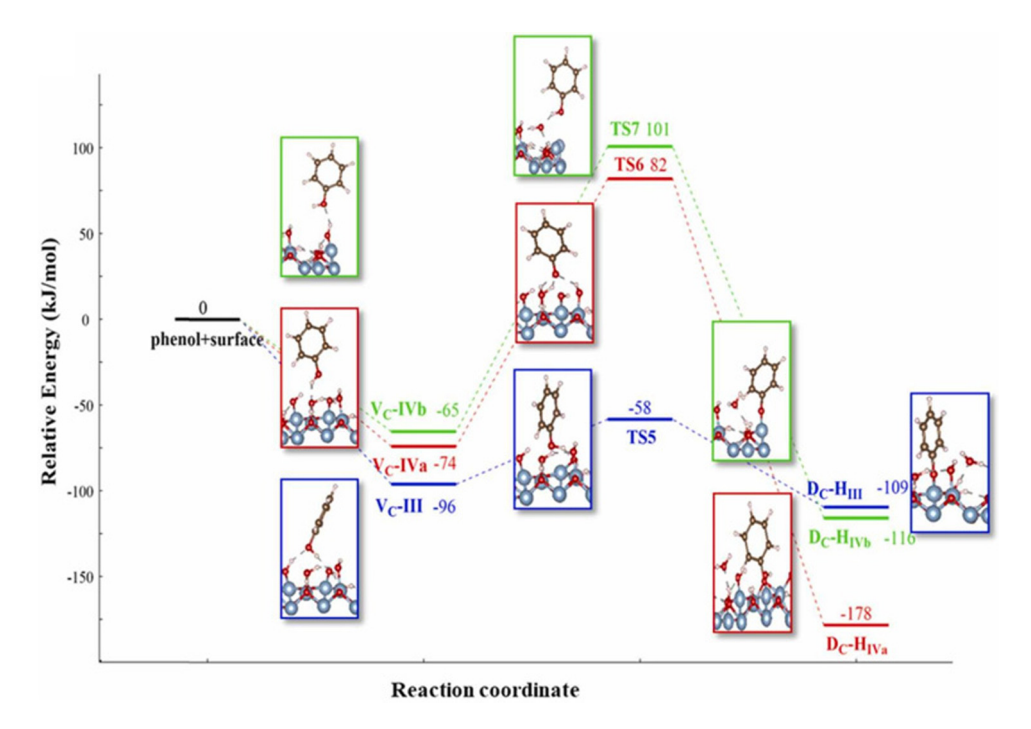


Figure 21: Formation mechanism of phenoxy-type EPFRs over hydroxylated alumina surfaces [138]. Reproduced with permission from Elsevier.

ortho/para-dihydroxylbenzenes), the effects of surface defects on the interaction of alumina with organic precursors for EPFRs, and the plausible role of silicate impurities in alumina. The formation of EPFRs from other substituted phenolic species, most notably, brominated phenols warrants a detailed investigation. These molecules emit invariably from the thermal decomposition of brominated flame retardants. With a significantly weaker aromatic C–Br bond in reference to C–Cl bond, bromine-bearing EPFRs may form in higher yields than their chlorinated counterparts. Likewise, it is also important to construct kinetic models that account for the temperature-dependent profiles of the generated EPFRs.

Funding information: This study was supported by a grant from the College of Engineering at the United Arab Emirates University via the Asian Universities Alliance (AUA) funding Scheme (UAEU, grant number: 12R174).

Author contributions: All authors have accepted responsibility for the entire content of this manuscript and approved its submission.

Conflict of interest: The authors state no conflict of interest.

Data availability statement: Data sharing is not applicable to this article as no datasets were generated or analysed during the current study.

References

- [1] Bolt A, Dincer I, Agelin-Chaab M. A review of unique aluminum-water based hydrogen production options. Energy Fuels. 2021;35:1024-40.
- [2] Pan B, Li H, Lang D, Xing B. Environmentally persistent free radicals: Occurrence, formation mechanisms and implications. Env Pollut. 2019;248:320–31.
- [3] Altarawneh M, Saeed A, Al-Harahsheh M, Dlugogorski BZ. Thermal decomposition of brominated flame retardants (BFRs): Products and mechanisms. Prog Energy Combust Sci. 2019;70:212–59.
- [4] Zhao J, Shen G, Shi L, Li H, Lang D, Zhang L, et al. Real-World emission characteristics of environmentally persistent free radicals in PM2.5 from residential solid fuel combustion. Env Sci Technol. 2022;56:3997–4004.
- [5] Wang Y, Li S, Wang M, Sun H, Mu Z, Zhang L, et al. Source apportionment of environmentally persistent free radicals (EPFRs) in PM_{2.5} over Xi'an, China. Sci Tot Env. 2019;689:193–202.
- [6] Ahmaruzzaman M. A review on the utilization of fly ash. Prog Energy Combust Sci. 2010;36:327-63.
- [7] Assaf NW, Altarawneh M, Oluwoye I, Radny M, Lomnicki SM, Dlugogorski BZ. Formation of environmentally persistent Free radicals on α -Al₂O₃. Env Sci Technol. 2016;50:11094–102.

- [8] Assaf NW, Altarawneh M, Oluwoye I, Radny M, Lomnicki SM, Dlugogorski BZ. Formation of phenoxy-Type EPFR over hydrated pure alumina and Si-Doped alumina surfaces. Organohalogen Compds. 2018;80:225–8.
- [9] Assaf NW, Altarawneh M, Radny MW, Al-Nu'airat J, Dlugogorski BZ. Formation of environmentally-persistent free radicals (EPFR) on α-Al₂O₃ clusters. RSC Adv. 2017;7:52672-83.
- [10] Liu Y, Oganov AR, Wang S, Zhu Q, Dong X, Kresse G. Prediction of new thermodynamically stable aluminum oxides. Sci Rep. 2015;5:9518.
- [11] Mousavi S, Abolhassani M, Hosseini M, Sebt S. Comparison of electronic and optical properties of the a and k phase alumina using density functional theory. Chin J Phys. 2009;48:862–73.
- [12] Hashimoto H, Onodera Y, Tahara S, Kohara S, Yazawa K, Segawa H, et al. Structure of alumina glass. Sci Rep. 2022;12:516.
- [13] Perevalov TV, Shaposhnikov A, Gritsenko VA, Wong H, Han J, Kim C. Electronic structure of α-Al₂O₃: Ab initio simulations and comparison with experiment. JETP Lett. 2007;85:165–8.
- [14] Wang B, Hou H, Luo Y, Li Y, Zhao Y, Li X. Density functional/ all-electron basis set slab model calculations of the adsorption/dissociation mechanisms of water on α -Al₂O₃ (0001) surface. J Phys Chem C. 2011;115:13399–411.
- [15] Wander A, Searle B, Harrison N. An ab initio study of α -Al₂O₃(0001): the effects of exchange and correlation functionals. Surf Sci. 2000;458:25–33.
- [16] Chang CC. LEED Studies of the (0001) Face of α -Alumina. J Appl Phys. 1968;39:5570–3.
- [17] French T, Somorjai GA. Composition and surface structure of the (0001) face of. alpha.-alumina by low-energy electron diffraction. J Phys Chem. 1970;74:2489-95.
- [18] Ahn J, Rabalais J. Composition and structure of the Al_2O_3 {0001}-(1 × 1) surface. Surf Sci. 1997;388:121–31.
- [19] Guenard P, Renaud G, Barbier A, Gautier-Soyer M. Determination of the α -Al $_2$ O $_3$ (0001) surface relaxation and termination by measurements of crystal truncation rods. MRS Online Proceedings Library Archive; 1996. p. 437
- [20] Toofan J, Watson P. The termination of the α -Al₂O₃(0001) surface: a LEED crystallography determination. Surf Sci. 1998:401:162–72.
- [21] Suzuki T, Hishita S, Oyoshi K, Souda R. Structure of α -Al₂O₃(0001) surface and Ti deposited on α -Al₂O₃ (0001) substrate: CAICISS and RHEED study. Surf Sci. 1999;437:289–98.
- [22] Manassidis I, Gillan MJ. Structure and energetics of alumina surfaces calculated from first principles. J Amer Chem Soc. 1994;77:335–8.
- [23] McHale J, Auroux A, Perrotta A, Navrotsky A. Surface energies and thermodynamic phase stability in nanocrystalline aluminas. Science. 1997;277:788-91.
- [24] Puchin V, Gale J, Shluger A, Kotomin E, Günster J, Brause M, et al. Atomic and electronic structure of the corundum (0001) surface: comparison with surface spectroscopies. Surf Sci. 1997;370:190–200.
- [25] Batyrev I, Alavi A, Finnis MW. Ab initio calculations on the Al₂O₃(0001) surface. Faraday Discuss. 1999;114:33-43.
- [26] Di Felice R, Northrup JE. Theory of the clean and hydrogenated Al_2O_3 (0001)–(1 \times 1) surfaces. Phys Rev B. 1999;60:R16287.

- [27] Verdozzi C, Jennison D, Schultz P, Sears M. Sapphire (0001) surface, clean and with d-metal overlayers. Phys Rev Lett. 1999;82:799.
- [28] Tepesch P, Quong A. First-principles calculations of α-alumina (0001) surfaces energies with and without hydrogen. Phys Status Solidi B. 2000;217:377–87.
- [29] Wang X-G, Chaka A, Scheffler M. Effect of the environment on α -Al₂O₃ (0001) surface structures. Phys Rev Lett. 2000;84:3650.
- [30] Tasker P. Surfaces of magnesia and alumina. Adv Ceram. 1984;10:176.
- [31] French RH, Heuer AH. International workshop on the science of alumina. J Amer Ceram Soc. 1994;77:292-2.
- [32] Manassidis I, De Vita A, Gillan MJ. Structure of the (0001) surface of α -Al₂O₃ from first principles calculations. Surf Sci. 1993;285:L517–21.
- [33] Kruse C, Finnis MW, Milman VY, Payne MC, Vita A, Gillan MJ. First-principles calculations for niobium atoms on a sapphire surface. J Amer Cera Soc. 1994;77:431–6.
- [34] Godin T, LaFemina JP. Atomic and electronic structure of the corundum (α-alumina)(0001) surface. Phys Rev B. 1994:49:7691.
- [35] Ballinger TH, Yates JT, Jr. Interaction and catalytic decomposition of 1, 1, 1-trichloroethane on high surface area alumina: An infrared spectroscopic study. J Phys Chem. 1992;96:1417–23.
- [36] Van Truong T, Kim DJ. Synthesis of high quality boehmite and γ-alumina for phosphorus removal from water works sludge by extraction and hydrothermal treatment. Env Res. 2022;212:113448.
- [37] Morterra C, Magnacca G. A case study: surface chemistry and surface structure of catalytic aluminas, as studied by vibrational spectroscopy of adsorbed species. Catal Today. 1996;27:497-532.
- [38] Lippens B, Linsen JSB, Fortuin M, Okkersee C, Steggerda J. Physical and chemical aspects of adsorbents and catalysts. London-New York: Acad. Press; 1970.
- [39] Peri JB, Hannan RB. Surface hydroxyl groups on γ-alumina. J Phys Chem. 1960;64:1526–30.
- [40] Peri J. A model for the surface of γ-alumina. J Phys Chem. 1965;69:220-30.
- [41] Cornelius E, Milliken T, Mills G, Oblad A. Surface strain in oxide cata1ysts -alumina. J Phys Chem. 1955;59:809-13.
- [42] Kasprzyk-Hordern B. Chemistry of alumina, reactions in aqueous solution and its application in water treatment. Adv Colloid Interface Sci. 2004;110:19–48.
- [43] Zhao Z, Xiao D, Chen K, Wang R, Liang L, Liu Z, et al. Nature of five-coordinated Al in γ-Al₂O₃ revealed by Ultra-high-field solid-state NMR. ACS CenSci. 2022;8:795–803.
- [44] Morris HD, Ellis PD. Aluminum-27 cross polarization of aluminas. The NMR spectroscopy of surface aluminum atoms.
 J Amer Chem Soc. 1989;111:6045-9.
- [45] Majors PD, Ellis PD. Surface site distributions by solid-state multinuclear NMR spectroscopy. Pyridine binding to.gamma.-alumina by nitrogen-15 and deuterium NMR. J Amer Chem Soc. 1987;109:1648-53.
- [46] Huggins BA, Ellis PD. Aluminum-27 nuclear magnetic resonance study of aluminas and their surfaces. J Amer Chem Soc. 1992;114:2098–108.
- [47] Coster D, Blumenfeld AL, Fripiat JJ. Lewis acid sites and surface aluminum in aluminas and zeolites: A high-resolution NMR study. J Phys Chem. 1994;98:6201–11.

- [48] Blumenfeld AL, Fripiat JJ. Acid sites topology in aluminas and zeolites from high-resolution solid-state NMR. Top Catal. 1997;4:119–29.
- [49] Lunsford JH. Characterization of acidity in zeolites and related oxides using trimethylphosphine as a probe. Top Catal. 1997;4:91–8.
- [50] Ripmeester JA. Surface acid site characterization by means of CP/MAS nitrogen-15 NMR. J Amer Chem Soc. 1983:105:2925-7.
- [51] Saito M, Aihara T, Miura H, Shishido T. Brønsted acid property of alumina-based mixed-oxides-supported tungsten oxide. Catal Today. 2021;375:64-9.
- [52] Webber J, Zorzi JE, Perottoni CA, Moura e Silva S, Cruz RCD. Identification of α -Al₂O₃ surface sites and their role in the adsorption of stearic acid. J Mater Sci. 2016;51:5170–84.
- [53] Tsyganenko A, Filimonov V. Infrared spectra of surface hydroxyl groups and crystalline structure of oxides. Spectrosc Lett. 1972;5:477-87.
- [54] Knöuzinger H. Specific poisoning and characterization of catalytically active oxide surfaces. Adv Catal. 1976;25:184–271.
- [55] Busca G, Lorenzelli V, Escribano VS, Guidetti R. FT-113 study of the surface properties of the spinels NiAl₂O₄ and CoAl₂O₄ in relation to those of transitional aluminas. J Catal. 1991;131:167-77.
- [56] Tsyganenko A, Filimonov V. Infrared spectra of surface hydroxyl groups and crystalline structure of oxides. J Mol Struct. 1973;19:579–89.
- [57] Knözinger H, Ratnasamy P. Catalytic aluminas: Surface models and characterization of surface sites. Catal Rev Sci. 1978;17:642.
- [58] Zaki M, Knözinger H. Carbon monoxide A low temperature infrared probe for the characterization of hydroxyl group properties on metal oxide surfaces. Mater Chem Phys. 1987;17:201–15.
- [59] Kung MC, Kung HH. IR studies of NH3, pyridine, CO, and NO adsorbed on transition metal oxides. Catal Rev Sci Eng. 1085-27-475-60
- [60] Brown GE, Henrich VE, Casey WH, Clark DL, Eggleston C, Felmy A, et al. Metal oxide surfaces and their interactions with aqueous solutions and microbial organisms. Chem Rev. 1999;99:77–174.
- [61] Desai R, Hussain M, Ruthven D. Adsorption of water vapour on activated alumina. I-equilibrium behaviour. Can J Chem Eng. 1992;70:699-706.
- [62] Rui Z, Yan Z, Kai H, Zhen-ping J, Gong-zhen C. NMR revealed activated alumina-water interaction. Wuhan Univ J Nat Sci. 2005;10:572-6.
- [63] Wang R, Zou Y, Remsing RC, Ross NO, Klein ML, Carnevale V, et al. Superhydrophilicity of α-alumina surfaces results from tight binding of interfacial waters to specific aluminols.
 J Colloid Interface Sci. 2022;628:943-54.
- [64] Coustet V, Jupille J. High-resolution electron-energy-loss spectroscopy of hydroxyl groups at the surface of bulk insulating oxides. Surf Interface Anal. 1994;22:280–3.
- [65] Elam JW, Nelson CE, Cameron MA, Tolbert MA, George SM. Adsorption of $\rm H_2O$ on a Single-Crystal α -Al $_2O_3(0001.)$ Surf J Phsy Chem B. 1998;102:7008–15.
- [66] McHale J, Navrotsky A, Perrotta A. Effects of increased surface area and chemisorbed H_2O on the relative stability of

- nanocrystalline γ -Al $_2$ O $_3$ and α -Al $_2$ O $_3$. J Phys Chem B. 1997;101:603–13.
- [67] Liu P, Kendelewicz T, Brown GE, Nelson EJ, Chambers SA. Reaction of water vapor with α -Al₂O₃ (0001) and α -Fe₂O₃ (0001) surfaces: synchrotron X-ray photoemission studies and thermodynamic calculations. Surf Sci. 1998;417:53–65.
- [68] Hass KC, Schneider WF, Curioni A, Andreoni W. The chemistry of water on alumina surfaces: Reaction dynamics from first principles. Science. 1998;282:265–8.
- [69] Hass K, Schneider W, Curioni A, Andreoni W. First-principles molecular dynamics simulations of H_2O on α -Al $_2O_3$ (0001). J Phys Chem B. 2000;104:5527–40.
- [70] Eng PJ, Trainor TP, Brown GE Jr, Waychunas GA, Newville M, Sutton SR, et al. Structure of the hydrated α -Al₂O₃ (0001) surface. Science. 2000;288:1029–33.
- [71] Al-Abadleh HA, Grassian V. FT-IR study of water adsorption on aluminum oxide surfaces. Langmuir. 2003;19:341-7.
- [72] Zhang L, Tian C, Waychunas GA, Shen YR. Structures and charging of α-alumina (0001)/water interfaces studied by sum-frequency vibrational spectroscopy. J Amer Chem Soc. 2008:130:7686-94.
- [73] Ranea VA, Schneider WF, Carmichael I. DFT characterization of coverage dependent molecular water adsorption modes on α -Al₂O₃(0001). Surf Sci. 2008;602:268–75.
- [74] Ranea VA, Carmichael I, Schneider WF. DFT investigation of intermediate steps in the hydrolysis of α -Al₂O₃ (0001). J Phys Chem C. 2009;113:2149–58.
- [75] Wittbrodt J, Hase W, Schlegel H. Ab initio study of the interaction of water with cluster models of the aluminum terminated (0001) α-aluminum oxide surface. J Phys Chem B. 1998;102:6539-48.
- [76] Shapovalov V, Truong TN. Ab initio study of water adsorption on α -Al₂O₃(0001) crystal surface. J Phys Chem B. 2000;104:9859–63.
- [77] Łodziana Z, Nørskov JK, Stoltze P. The stability of the hydroxylated (0001) surface of α-Al₂O₃. J Chem Phys. 2003;118:11179–88.
- [78] Gaigeot M-P, Sprik M, Sulpizi M. Oxide/water interfaces: how the surface chemistry modifies interfacial water properties. J Phys Condens Matter. 2012;24:124106.
- [79] Braunschweig B, Eissner S, Daum W. Molecular Structure of a Mineral/Water Interface: Effects of Surface NanoRoughness of α -Al₂O₃ (0001). J Phys Chem C. 2008;112:1751–4.
- [80] Flörsheimer M, Kruse K, Polly R, Abdelmonem A, Schimmelpfennig B, Klenze R, et al. Hydration of mineral surfaces probed at the molecular level. Langmuir. 2008;24:13434-9.
- [81] Sung J, Zhang L, Tian C, Shen YR, Waychunas GA. Effect of pH on the water/ α -Al₂O₃ (1102) interface structure studied by sum-frequency vibrational spectroscopy. J Phys Chem C. 2011;115:13887–93.
- [82] Sung J, Shen Y, Waychunas G. The interfacial structure of water/protonated α-Al₂O₃ as a function of pH. J Phys Condens Matter. 2012;24:124101.
- [83] Huang P, Pham TA, Galli G, Schwegler E. Alumina (0001)/ water interface: structural properties and infrared spectra from first-principles molecular dynamics simulations. J Phys Chem C. 2014;118:8944–51.
- [84] Mawhinney DB, Rossin JA, Gerhart K, Yates JT. Adsorption and reaction of 2-chloroethylethyl sulfide with Al₂O₃ surfaces. Langmuir. 1999;15:4789-95.

- [85] Ludwig B, Burke TT. Infrared spectroscopy studies of aluminum oxide and metallic aluminum powders, Part I: Thermal dehydration and decomposition. Powders. 2022;1:47–61. doi: 10.3390/powders1010005
- [86] Nelson C, Elam J, Cameron M, Tolbert M, George S. Desorption of H₂O from a hydroxylated single-crystal α-Al₂O₃(0001) surface. Surf Sci. 1998;416:341-53.
- [87] Hendriksen BA, Pearce DR, Rudham R. Heats of adsorption of water on α- and γ-alumina. J Catal. 1972;24:82-7.
- [88] Medema J. Isomerization of butene over alumina. J Catal. 1975;37:91–100.
- [89] Ballinger TH, Yates JT Jr. High-temperature behavior of rhodium/alumina catalysts. J Phys Chem. 1991;95:1694–8.
- [90] Wischert R, Copéret C, Delbecq F, Sautet P. Dinitrogen: a selective probe for tri-coordinate Al "defect" sites on alumina. Chem Comm. 2011;47:4890-2.
- [91] Joubert J, Salameh A, Krakoviack V, Delbecq F, Sautet P, Copéret C, et al. Heterolytic splitting of H₂ and CH₄ on γ-alumina as a atructural probe for defect sites. J Phys Chem B. 2006;110:23944–50.
- [92] Wischert R, Copéret C, Delbecq F, Sautet P. Optimal Water Coverage on Alumina: A key to generate lewis acid-base pairs that are reactive towards the C-H bond activation of methane. Angew Chem Int Ed. 2011;50:3202-5.
- [93] Zambon P, Ricci P, Bovo E, Casula A, Gattolin M, Fiore AR, et al. Sarcoma risk and dioxin emissions from incinerators and industrial plants: a population-based case-control study (Italy). Env Health. 2007;6:19.
- [94] Floret N, Lucot E, Badot P-M, Mauny F, Viel J-F. A municipal solid waste incinerator as the single dominant point source of PCDD/Fs in an area of increased non-Hodgkin's lymphoma incidence. Chemosphere. 2007;68:1419–26.
- [95] Sioutas C, Delfino RJ, Singh M. Exposure assessment for atmospheric ultrafine particles (UFPs) and implications in epidemiologic research. Env Health Perspect. 2005;113:947.
- [96] Ntziachristos L, Froines JR, Cho AK, Sioutas C. Relationship between redox activity and chemical speciation of size-fractionated particulate matter. Part Fibre Toxicol. 2007;4:5.
- [97] Zhu Y, Hinds WC, Kim S, Sioutas C. Concentration and size distribution of ultrafine particles near a major highway. J Air Waste Manag Assoc. 2002;52:1032–42.
- [98] Barmpadimos I, Keller J, Oderbolz D, Hueglin C, Prévôt A. One decade of parallel fine (PM 2.5) and coarse (PM 10-PM 2.5) particulate matter measurements in Europe: trends and variability. Atmos Chem Phys. 2012;12:3189-203.
- [99] Cusack M, Alastuey A, Pérez N, Pey J, Querol X. Trends of particulate matter (PM 2.5) and chemical composition at a regional background site in the Western Mediterranean over the last nine years (2002–2010). Atmos Chem Phys. 2012;12:8341–57.
- [100] Bølling AK, Pagels J, Yttri KE, Barregard L, Sallsten G, Schwarze PE, et al. Health effects of residential wood smoke particles: the importance of combustion conditions and physicochemical particle properties. Part Fibre Toxicol. 2009;6:29.
- [101] Dellinger B, Pryor WA, Cueto R, Squadrito GL, Hegde V, Deutsch WA. Role of free radicals in the toxicity of airborne fine particulate matter. Chem Res Toxicol. 2001;14:1371-7.
- [102] Walsh M, Cormier S, Varner K, Dellinger B. By-products of the thermal treatment of hazardous waste: Formation and health effects. EM (Pittsburgh, Pa). 2010;26:1–8.

- [103] Dellinger B, Lomnicki S, Khachatryan L, Maskos Z, Hall RW, Adounkpe J, et al. Formation and stabilization of persistent free radicals. Proc Combust Inst. 2007;31:521–8.
- [104] Lomnicki S, Truong H, Vejerano E, Dellinger B. Copper oxidebased model of persistent free radical formation on combustion-derived particulate matter. Env Sci Technol. 2008;42:4982-8.
- [105] Peters A, Dockery DW, Muller JE, Mittleman MA. Increased particulate air pollution and the triggering of myocardial infarction. Circulation. 2001;103:2810-5.
- [106] Nel A. Air pollution-related illness: effects of particles. Science. 2005;308:804-6.
- [107] Vejerano E, Lomnicki S, Dellinger B. Formation and stabilization of combustion-generated environmentally persistent free radicals on an Fe(III)₂O₃/silica surface. Env Sci Technol. 2010;45:589-94.
- [108] Vejerano E, Lomnicki SM, Dellinger B. Formation and stabilization of combustion-generated, environmentally persistent radicals on Ni (II)O supported on a silica surface. Env Sci Technol. 2012;46:9406-11.
- [109] Cass GR, Hughes LA, Bhave P, Kleeman MJ, Allen JO, Salmon LG. The chemical composition of atmospheric ultrafine particles. Philos Trans R Soc A. 2000;358:2581–92.
- [110] Patterson MC, Keilbart ND, Kiruri LW, Thibodeaux CA, Lomnicki S, Kurtz RL, et al. EPFR formation from phenol adsorption on Al₂O₃ and TiO₂: EPR and EELS studies. Chem Phys. 2013;422:277–82.
- [111] Farquar GR, Alderman S, Poliakoff E, Dellinger B. X-ray spectroscopic studies of the high temperature reduction of Cu (II)O by 2-chlorophenol on a simulated fly ash surface. Env Sci Technol. 2003;37:931–5.
- [112] Alderman S, Farquar GR, Poliakoff E, Dellinger B. Reaction of 2-chlorophenol with CuO: XANES and SEM analysis. Proc Combust Inst. 2005;30:1255-61.
- [113] Patterson MC, Thibodeaux CA, Kizilkaya O, Kurtz RL, Poliakoff E, Sprunger PT. Electronic Signatures of a Model Pollutant-Particle System: Chemisorbed Phenol on TiO₂ (110). Langmuir. 2015;31:3869-75.
- [114] Vejerano E, Lomnicki S, Dellinger B. Lifetime of combustiongenerated environmentally persistent free radicals on Zn(II)O and other transition metal oxides. J Env Monit. 2012;14:2803-6.
- [115] Mosallanejad S, Dlugogorski BZ, Kennedy EM, Stockenhuber M, Lomnicki SM, Assaf NW, et al. Formation of PCDD/Fs in oxidation of 2-chlorophenol on neat silica surface. Env Sci Technol. 2016;50:1412-8.
- [116] Altarawneh M, Dlugogorski BZ. Formation and chlorination of carbazole, phenoxazine, and phenazine. Env Sc Technol. 2015;49:2215–21.
- [117] Altarawneh M, Dlugogorski BZ. Formation of dibenzofuran, dibenzo-p-dioxin and their hydroxylated derivatives from catechol. Phys Chem Chem Phys. 2015;17:1822-30.
- [118] Altarawneh M, Radny MW, Smith PV, Mackie JC, Kennedy EM, Dlugogorski BZ, et al. A first-principles density functional study of chlorophenol adsorption on Cu₂O (110): CuO. J Chem Phys. 2009;130:184505.
- [119] Altarawneh M, Carrizo D, Ziolkowski A, Kennedy EM, Dlugogorski BZ, Mackie JC. Pyrolysis of permethrin and formation of precursors of polychlorinated dibenzo-p-dioxins

- and dibenzofurans (PCDD/F) under non-oxidative conditions. Chemosphere. 2009;74:1435–43.
- [120] Altarawneh M, Dlugogorski BZ, Kennedy EM, Mackie JC. Quantum chemical study of low temperature oxidation mechanism of dibenzofuran. J Phys Chem A. 2006;110:13560–7.
- [121] Altarawneh M, Dlugogorski BZ, Kennedy EM, Mackie JC. Theoretical study of reaction pathways of dibenzofuran and dibenzo-p-dioxin under reducing conditions. J Phys Chem A. 2007;111:7133-40.
- [122] Altarawneh M, Kennedy EM, Dlugogorski BZ, Mackie JC. Computational study of the oxidation and decomposition of dibenzofuran under atmospheric conditions. J Phys Chem A. 2008:112:6960-7.
- [123] Altarawneh M, Radny MW, Smith PV, Mackie JC, Kennedy EM, Dlugogorski BZ. Adsorption of chlorophenol on the Cu(111) surface: A first-principles density functional theory study. Appl Surf Sci. 2008;254:4218-24.
- [124] Lomnicki S, Truong H, Dellinger B. Mechanisms of product formation from the pyrolytic thermal degradation of catechol. Chemosphere. 2008;73:629-33.
- [125] Truong H, Lomnicki S, Dellinger B. Mechanisms of molecular product and persistent radical formation from the pyrolysis of hydroquinone. Chemosphere. 2008;71:107–13.
- [126] Takasuga T, Makino T, Tsubota K, Takeda N. Formation of dioxins (PCDDs/PCDFs) by dioxin-free fly ash as a catalyst and relation with several chlorine-sources. Chemosphere. 2000;40:1003-7.
- [127] Seames WS. An initial study of the fine fragmentation fly ash particle mode generated during pulverized coal combustion. Fuel Process Technol. 2003;81:109-25.
- [128] Cains PW, McCausland LJ, Fernandes AR, Dyke P. Polychlorinated dibenzo-p-dioxins and dibenzofurans formation in incineration: effects of fly ash and carbon source. Env Sci Technol. 1997;31:776–85.
- [129] Guan X, Ghimire A, Potter PM, Lomnicki SM. Role of Fe₂O₃ in fly ash surrogate on PCDD/Fs formation from 2-monochlorophenol. Chemosphere. 2019;226:809-16.
- [130] Potter PM, Dellinger B, Lomnicki SM. Contribution of aluminas and aluminosilicates to the formation of PCDD/Fs on fly ashes. Chemosphere. 2016;144:2421-6.
- [131] Pan W, Zhong W, Zhang D, Liu C. Theoretical study of the reactions of 2-chlorophenol over the dehydrated and hydroxylated silica clusters. J Phsy Chem A. 2011;116:430-6.
- [132] Mosallanejad S, Dlugogorski BZ, Altarawneh M, Kennedy EM, Yokota M, Nakano T, et al. Decomposition of 2-chlorophenol on surfaces of neat alumina and alumina supported iron (III) oxide catalysts. Organohalogen Compds. 2014;76:396–9.
- [133] Yang L, Liu G, Zheng M, Jin R, Zhao Y, Wu X, et al. Pivotal roles of metal oxides in the formation of environmentally persistent free radicals. Env Sci Technol. 2017;51:12329–36.
- [134] Ye Y, Li Y, Wang J, Yuan S, Xu X, Zhang X, et al. Generation of environmentally persistent free radicals on metal-organic frameworks. Langmuir. 2022;38:3265-75.
- [135] Liu S, Liu G, Yang L, Liu X, Wang M, Qin L, et al. Metal-catalyzed formation of organic pollutants intermediated by organic free radicals. Env Sci Technol. 2022;20:14550-61.
- [136] Chen ZX, Li Y, Huang F. Persistent and stable organic radicals: design, synthesis, and applications. Chem. 2021;7:288-332.

- [137] Liu S, Liu G, Yang L, Li D, Zheng M. Critical influences of metal compounds on the formation and stabilization of environmentally persistent free radicals. Chem Eng J. 2022;427:131666.
- [138] Wang W, Zhang R, Liu Z, Wang W, Zhang Q, Wang Q. Periodic DFT calculation for the formation of EPFRs from phenol on
- γ -Al₂O₃ (110): Site-dependent mechanism and the role of ambient water. J Env Chem Eng. 2022;10:108386.
- [139] De S, Saha B, Luque R. Hydrodeoxygenation processes: Advances on catalytic transformations of biomass-derived platform chemicals into hydrocarbon fuels. Bioresour Technol. 2015;178:108-18.